RIVISTA DEL NUOVO CIMENTO Vol. 40, N. 5 2017
DOI 10.1393/ncr/i2017-10135-7

The structure of DNA by direct imaging and related topics

M. Marini, T. Limongi, M. Moretti, L. Tirinato and E. Di Fabrizio

King Abdullah University of Science and Technology, PSE and BESE Divisions
Thuwal, 23955-6900, Kingdom of Saudi Arabia

received 15 December 2016

Summary. — Super-hydrophobicity is a well-known and studied phenomenon in the field of surface sciences. In this review we report a novel approach that exploits micro-fabricated super-hydrophobic surfaces for the oriented and self-organized deposition and suspension of DNA filaments and other macromolecules of biological interest. The self-assembled structures obtained with this approach can be used for the characterization of the biological compounds with several methods such as electron microscopy, X-ray diffraction, Raman and SERS spectroscopies. Besides imaging, the described method has been applied in several fields such as the sensing of few molecules in diluted solutions and innovative templating growth. We will focus in particular on the direct imaging of DNA molecules by Transmission Electron Microscopy with the capability to resolve structural details of the double helix down to a resolution of 1.5 Å. The review starts with a brief historical note on the discovery of the DNA structure and continues with the results obtained by our group along the last 10 years of activity.

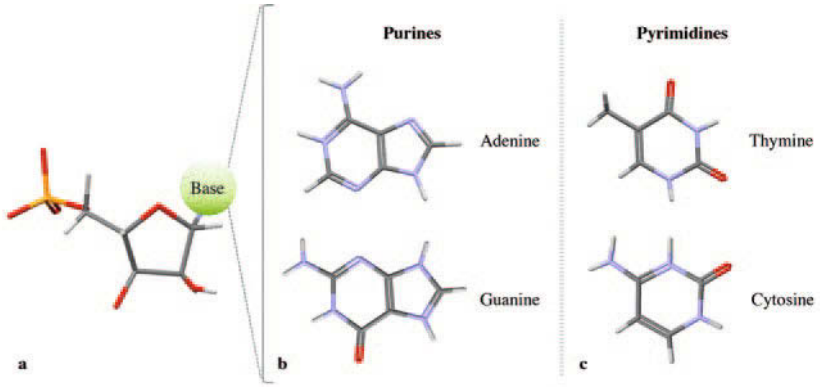

Fig. 1. – Nucleotides, the DNA monomers, are composed of three main parts: a phosphate group, a 5-atoms carbon sugar and a nitrogenous base (a). The first attempt to give a correct order to these three moieties was performed by Leven in the early 1900s but it is only in the 50s that the four bases where distinguished and divided in (b) purines (A, G) and pyrimidines (T, C) (c).

1. – DNA: from the 1860s to "Photo 51"

The story of the DNA starts in 1869, when the Swiss physiological chemist Friedrich Miescher identified the "nuclein" while working with human leukocites (white blood cells). In its attempt to isolate and characterize the proteic component of the white blood cells, he discovered a new substance; what he called "nuclein" nowadays is known as nucleic acid, deoxyribonucleic acid or, with its acronym, DNA.

50 years later the Lituan physician and chemist Phoebus Levene, pointed out that that the nucleic acids have a sugar component: the ribose, discovered in 1909 [1] or the deoxyribose (1929) [2]. Levene by working on the hydrolysis on nucleic acids extracted from yeast, suggested that DNA is constituted by nucleotides, each one formed by one of the four bases containing nitrogen, a carbohydrate-based component, and a phosphate. Levene contributed to give a proper order to the three DNA backbone building blocks, proposing the correct spatial sequence phosphate-sugar-base.

In 1944 Avery, McLeod and McCarty demonstrated that inheritage is driven by genes, which are DNA fragments [3]. This achievement inspired the Austrian biochemist Erwin Chargaff to investigate the chemical properties and features of nucleic acids. He isolated and fractionated DNA from cells nuclei using an optimized paper chromatography method, suitable for the separation of small organic molecules. He separated two substances on the basis of their solubility, solving the two types of bases: purines (A and G) and pyrimidines (T and C). The extracted substances were then exposed to UV light and the differences in absorption allowed determining the quantity of each base present in the tested DNA. Chargaff concluded that DNA base sequences vary among the belonging strands but some rules on the DNA composition remain fixed: no matter which specie was tested, the amounts of adenine (A) and thymine (T) are similar and the same happens for the amounts of cytosine (C) and guanine (G). The total amount of pyrimidines and the total amount of purines are usually very close to each other; this became a rule named "Chargaff's rule" (1950s) that strongly contributed years later to the final determination of the DNA structure (fig. 1) [4].

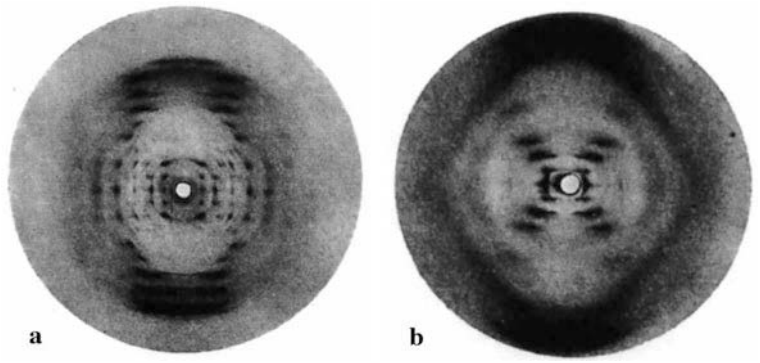

Fig. 2. – X-ray diffraction patterns for the two forms of DNA: (a) A-form and (b) B-form. Readapted from [8].

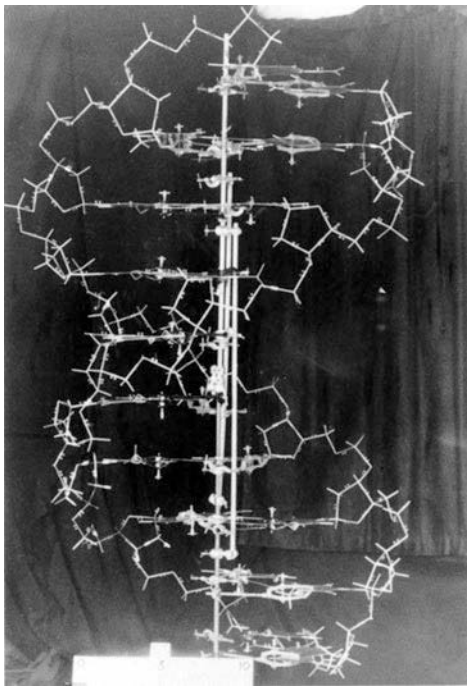

Fig. 3. – Watson and Crick's original 3-D demonstration model of DNA.

Among the physical methods, X-Ray diffraction had the most important role in obtaining structural information about the polynucleotide. It was in 1952 that Rosalind Franklin, Maurice Wilkins and Raymond Gosling took two sets of high-resolution photos of crystallized DNA fibers from calf thymus. In presence of a humidity lower than 75%, the fiber showed an X-Ray diagram as a scatter with distinct spots. The X-ray pattern turned in to a striking X shape [5-8] while the addition of the moisture to the atmosphere allowed a humidity over 75%. This "X-shaped" feature, characterized in 1950 by Linus Pauling and identified as the α-helix secondary structure of proteins [9], was suggesting

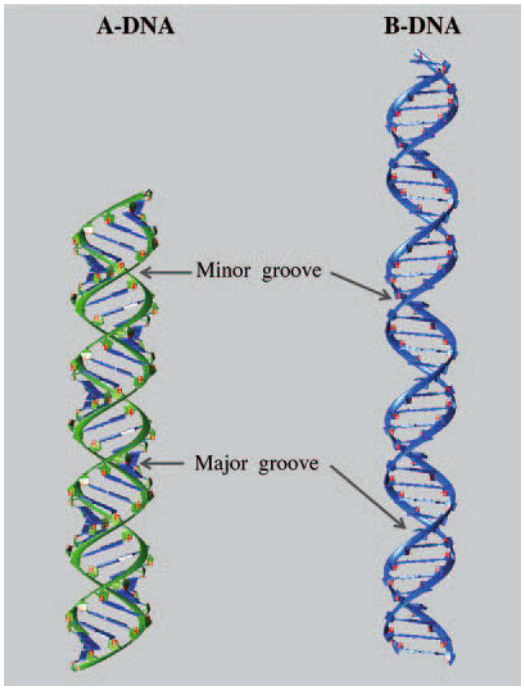

Fig. 4. – Models of a DNA double helix in the A- (in green) and the B- (in blue) form. Forty arbitrary bases extracted from the λ-DNA sequence were used to simulate the DNA in the A- and B-forms (left and right, respectively). The hydration state (less than 75% in the A-form, higher than 75% in the B-form) affects period length, diameter of the helix, tilt of the bases and turn of the helix.

that DNA was arranged as a helix as well. In addition, the two patterns demonstrated the existence of two possible DNA conformations: the A-form and the B-form. The A-form, obtained with humidity lower than 75%, can be reverted to the B-form changing the molecule hydration status and increasing the humidity over 75%. This interchange represents an adaptation of the DNA conformation to the environment, without effects on the bio-chemistry of the polynucleotide (fig. 2).

The X-Ray pattern of B-DNA, known as "Photo 51", provided fundamental information on the double-helix arrangement and its dimensions. It strongly helped James Watson and Francis Crick in the interpretation and finalization of the helical structure of B-DNA [10] (fig. 3). Watson, Crick and Wilkins deserved the Nobel Prize in Physiology and Medicine for the elucidation of the DNA structure in 1962.

The diffraction pattern interpretation determined the right-handed helical behavior of the double-strand DNA and the characterization of its chemical arrangement as well. The two hemi-helices of the double-strand DNA are anti-parallel, complementary and kept in position by the hydrogen bonds naturally occurring between purines and pyrimidines. Adenine is always paired with Thymine while Cytosine is always paired with Guanine, as previously stated in Chargaff's rule. The diameter of a helix in the B-form is around 20 Å, with an interbases distance of 3.4 Å and, consequently, a pitch of 34 Å. The less hydrated A-DNA form has a shorter pitch of 28.2 Å with an interbase distance reduced to 2.56 Å (fig. 4). Detailed experimental measures on both conformations are reported in table I. Despite the pivotal role of X-Ray diffraction in the achievement of the correct

TABLE I. – *X-Ray accepted values for the main features of A- and B-DNA.*

	Structural characteristics[(a)]	
Features	A-DNA (Å)	B-DNA (Å)
Diameter	23	20
Rise/BP along axis	2.56	3.4
Pitch/turn of helix	28.2	34
BP/turn	11	10.4
Minor groove	Wide	Narrow
Major groove	Narrow	Wide
Coils	Right-handed	Right-handed
Tilt of base pair relative to the axis	19°	−6°

[(a)] X-Ray accepted values as reported in [8, 13, 14].

structure of double-strand B-DNA, this worldwide known technique [11] faces critical limitations. First, a crystal has to be obtained. It could require several months of work [12] to reduce the desired molecule into crystals large enough to be suitable for the downstream analysis and to cope with the repeated exposure to the X-Ray beam. The starting material has to be extremely pure and of high quality and not all the biological materials can successfully undergo to the crystallization process. Even though it has been applied to most of the macromolecules of interest in biology, X-Ray crystallography gives information only on the crystal configuration state as a function of the environment, not on single molecules.

2. – DNA structural characterization: current methods

After its discovery the research related to DNA had an enormous break through. Despite the constant advances, there is still a strong need to improve the techniques for structural studies at atomic resolution that spans from cellular and molecular biology, genomics to the modern translational medicine research. Substantial improvements in the characterization of the nano- and sub-nanoscale arrangement of molecular aggregates, nucleic acids, transcription factors, repressor and activator proteins [15-17] are still object of investigation. The elaboration of methods for the direct imaging of DNA is strongly required since the diffusion of a wide range of native and synthetic nucleic acid in therapeutic and drug delivery application. In details, DNA-based Therapeutics (DbT) include plasmid-based [18], oligonucleotides for antisense applications [19, 20] and aptamers [21] solutions. Aptamers, double-stranded nucleic acid, by interacting with proteins, have been broadly used as therapeutic mediators for the diagnosis and care of human illnesses, the Macugen has been just approved for age-related macular degeneration [22] and other aptamers are under evaluation for coagulation, oncology and inflammation applications [23, 24]. Advanced techniques for high-resolution background-free DNA visualization are highly desired also for the study of circulating tumor DNA (ctDNA) and circulating cell-free DNAs such as mitochondrial DNA [25, 26].

In this context we propose a novel approach devoted to the direct imaging of DNA. The method consists in the combination of the super-hydrophobic properties of a micro-

fabricated surface and the spontaneous self-assembly that is driven by the device texture. Due to the low friction coefficient characterizing such surfaces, they can be efficiently used to manipulate solutions containing the molecules object of investigation. A drop of the sample is deposited over the super-hydrophobic device and is let to evaporate until it is completely dry. The moieties diluted in the solution become more and more concentrated in a defined area while the dehydration process occurs. This mechanism allows reducing a starting solution containing floating DNA molecules into oriented and self-aligned bundles constituted by nucleic acid helices, suspended between the micro asperities of the devices. The concurrent self-alignment and the particular architecture achieved by the DNA helices, made them suitable for direct imaging in background-free condition with the potential to achieve an unprecedented resolution of 1.5 Å. The approach as well as the devices were conveniently modified from case to case, widening the range of applicability from detection in diluted solutions to biomolecules characterization by means of X-Ray diffraction, Raman spectroscopy and electron microscopy. The details on the suspension and imaging method as well as the other applications are reported in detail in the next sections.

In this section we focus on the most common methods used to image and characterize macromolecules such as nucleic acids and proteins, pointing out the most recent achievements in the techniques presented and the related limits.

2˙1. *Optical methods.* – Optical methods used to visualize nucleic acids usually demand systems labeling DNA-associated proteins or the use of small flag and nanoparticles that could affect the native configuration and function [27]. Most efficient techniques are required for viewing cellular components such as nucleic acids and chromatin in their original conformation without the use of fluorophores or labels as required for most of the super-resolution techniques as stochastic optical reconstruction, stimulated emission depletion and photo-activated localization microscopy [28, 29]. Sample preparation for super-resolution microscopy techniques commonly uses different kinds of nucleic acids conjugated-proteins [30] for indirect imaging of DNA, chromatin and condensed mitotic chromosome structure at nanometer resolution [31].

2˙2. *Scanning probes: Atomic Force Microscopy (AFM) and Scanning Tunneling Microscopy (STM).* – Since 1990s, AFM applied to biomolecules is a growing field. As DNA is a material relatively easy to find, it has been widely used for AFM imaging and non-imaging applications. AFM remains unique in its capability to provide height information on samples and details on soft materials. The biopolymers dispersed in a liquid solution have to be deposited on an atomically flat substrate (*i.e.* muscovite mica) and the imaging can be performed in air (after complete sample drying) or in liquid [32].

The force sensitivity and its control have a central role in high-resolution AFM imaging as it can cause sample deformation. The preparation needed is not straightforward as well. The sample has to be immobilized on the substrate, procedure that usually needs the use of salts containing mono- or di-valent cations (*i.e.* Mg^{2+}, Ni^{2+}). In both cases, imaging resolution can be severely compromised and lead to misleading data interpretation.

AFM performed in fluid allowed reaching a molecular resolution down to approximately 1 nm of spatial resolution, attracting the attention of biologists interested in elucidating systems behaviors in their physiological environment. In the plethora of the nanoscale imaging techniques, AFM is an effective tool, characterized by less invasive sample preparation without the need of heavy treatments as in standard Electron Mi-

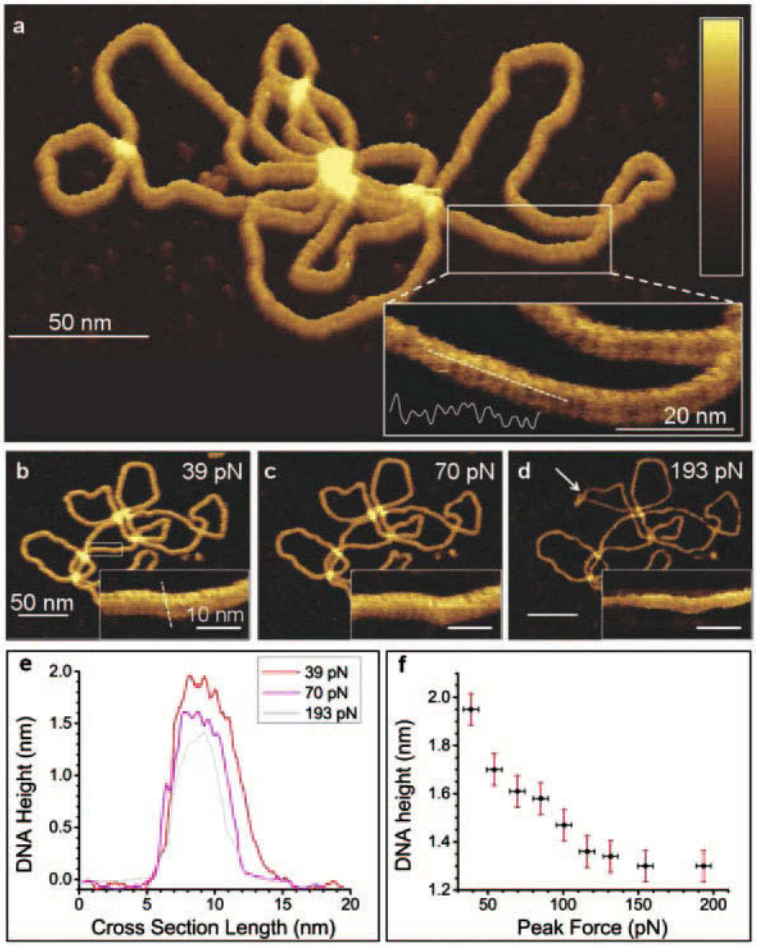

Fig. 5. – AFM topographic images of a DNA plasmid, captured in rapid force-distance mode in a buffer solution containing Ni^{2+} as divalent cation. (a-d) Three forces were applied for imaging and the corrugations along the double helix, corresponding to the major and minor grooves, are evidenced in the insets. (e, f) The forces applied affect the measured height and diameter of the double strand. Reprinted from [38]. © 2014 The Authors. Published by WILEY-2010VCH Verlag GmbH & Co. KGaA, Weinheim.

croscopy analyses. Further, AFM demonstrated some success in static and dynamics characterization of DNA and DNA/protein complexes [33-37]. A few examples of imaging resolution, enough to solve some of the main features of dsDNA, have been recently reported [38-40]. Hoogenboom's research group used miniaturized cantilevers to image DNA grooves depth related to the molecule in the B-form. Major and minor groove were solved but the helix width was overestimated by 7–10 nm (fig. 5).

In recent years scanning tunneling microscopy (STM) has been used to examine a DNA sequence and to localize individual bases along the molecule. In STM, a voltage is applied between a fine metallic AFM tip and a conductive substrate over which the imaging scan is performed. A current (the "tunneling current") can flow when the tip is at a "tunnel" distance (few Å) from the molecule; under the proper conditions the

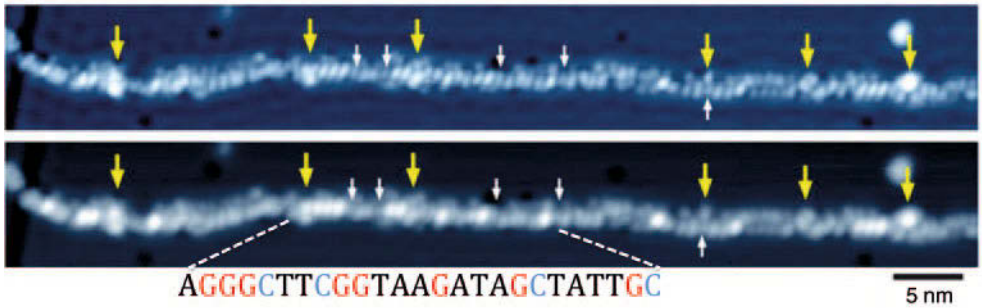

Fig. 6. – Bias voltage dependence on the STM imaging of M13mp18 DNA on a Cu(111) surface. (a-b) Raw data at different bias voltage in which the guanine bases result as bright and distinct features along the strand and (c) correspondent M13mp18 sequence from nucleotide 2911 to nucleotide 3011. White arrows indicate cytosine and yellow arrows the presence of contaminants. Reprinted from [41], © 2009, Rights Managed by Nature Publishing Group.

topographic maps of the molecules fixed on the surface can be achieved. An attempt of nucleic acid sequencing has been reported in 2009 in the work of Tanaka and Kawai [41], where STM imaging and Scanning Tunneling Spectroscopy (STS) [42] were combined to investigate single-strand DNA molecules adsorbed over a copper substrate. Along the strand, the guanine base showed a characteristic electronic state that resulted in a larger and brighter detail in the acquired images (fig. 6). The other bases were not identified but knowing the used sequence, the researcher where able to guess the correspondence between the partially sequenced strand and the real bases of the hemi-helix.

Conformational changes such as bending and molecule/molecule interaction can be detected with these techniques. AFM was successfully used to investigate the DNA/protein conformational changes as in the case of the MutS protein family. MutS has a weak ATPase activity and it is involved in the repair of mismatches along a DNA sequence, fundamental mechanism at the basis of genomic stability. MutS firstly recognizes the mismatch on the DNA sequence then, upon ATP hydrolysis, bends the nucleic acid provoking a unique conformational change leading the cascade of subsequent genomic reparation events. By means of AFM technique, researchers clarified the non-specificity of the initial DNA binding —and pointed out that the specificity is fundamental for the single-base mismatch recognition event [43], causing the protein conformational changes [44]. The MutS action mechanism has been further elucidated in 2011, when AFM images distinguished the MutS/DNA single-site binding and loop-binding complexes, driving to the conclusion that MutS protein can act in a tetrameric conformation [45].

2˙3. *Transmission Electron Microscopy (TEM).* – Biological material can be visualized by TEM to produce 2-D images of an object. The negative and positive staining is a widely used practice in imaging biological materials [46]; electron-dense heavy-atoms such as lead citrate, osmium tetroxide and uranyl acetate, are dissolved in salt solutions and then applied to enhance the contrast of the specimen. In negative staining, the objects appear brighter than the stained background; vice versa, in positive staining, the specimen interacts directly with the stain and becomes darker than the background. Most of the biological studies involve the use of grids with a mesh size chosen on the basis of the application. On top of the grid a thin carbon layer is deposited by evaporation of carbon graphite to allow the sample adhesion.

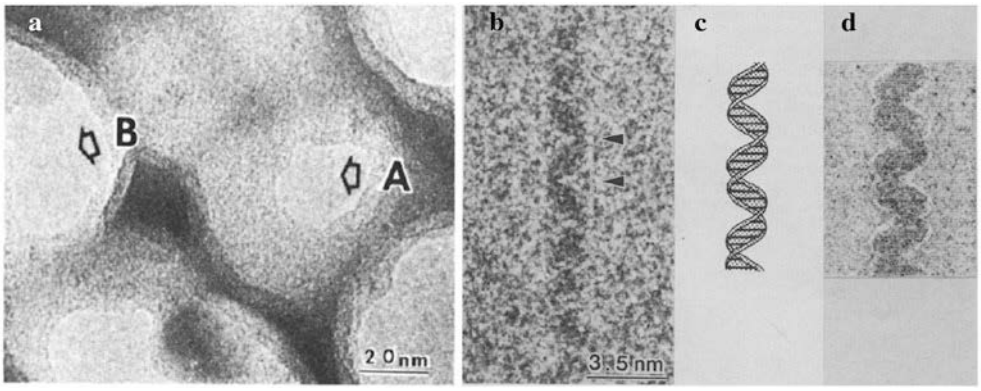

Fig. 7. – (a) Unstained single molecules of double-strand DNA hanging over the holes of a super-microgrid are indicated by the arrows. (b) Enlarged image of the fiber indicated with arrow A in panel (a), resembling the Watson-Crick DNA model (c) and the theoretical model (d). Readapted from [48]. © 1981 Published by Elsevier B.V.

In light molecular weight samples, high-resolution imaging with conventional support systems and staining solutions cannot be achieved because the supporting film absorbs and scatters the electron beam, producing a pretty strong background signal that interferes with the fine details of the sample. To overcome this limitation, the group of Uyeda prepared alumina super-microgrids (ASM) provided with holes (20–100 nm diameter) [47] across which the DNA molecules hang without any carbon layer support. This allowed the authors to obtain a molecular image of a freeze-dried DNA in the B-form, accordingly to Watson-Crick model and to the computer simulations [48]. The improved signal-to-noise ratio let the visualization of the double-helix features. Major and minor grooves were recognized and two lengths were measured: the width of 2 nm and the pitch of 3.5 nm (fig. 7).

2˙4. *Cryo Electron Microscopy (Cryo-EM).* – The use of cryo-EM started in the 1974 with the works on "electron diffraction of frozen, hydrated protein crystals" [49]. Its extensive application in structural biology arised only after the recent technical advances in microscopy such as the development of direct electron detectors, the beam-induced motion correction [50], the computing clusters and 3-D image reconstructions [51, 52]. Briefly, the sample is flash-frozen at a temperature of $-180°$ so that the objects under analysis are randomly distributed with a random orientation in a layer of glass-like ice. Thousands of 2-D projections of the object at different angles have to be acquired and subsequently sorted and averaged by dedicated algorithms to reconstruct a final 3-D structure [53].

Recently, resolutions ranging between 2.2 and 3 Å were achieved for protein complexes or single proteins with high molecular weight. A 2.2 Å resolution was achieved in the study of a complex between *E. coli* β-galactosidase and an inhibitor [54]. A year after a 2.3 Å resolution for the structure of p97 ATPase was determined using similar strategies [55]. Compared to X-ray crystallography, Cryo-EM shows major advantages as it does not need the preliminary preparation of a 3-D crystal, but faces other limitations. The number of images needed for the downstream reconstructions results in tens or hundreds of imaged particles that have to be properly aligned before averaging, process

that is severely affecting the quality of the final result. Furthermore, the low signal-to-noise ratio, the resolution limited by the hydrated state of the frozen sample [56], its relative "un-phisiological state", and the beam-induced motion correction are still under discussion [57, 58].

Despite all the technical advances and the improvements in the preparation techniques, cryo-EM still lacks of atomic resolution in particular for molecules and complexes small in size, transient or asymmetric. The application of cryo-EM to single DNA molecules, in fact, is still missing and the only achievements on these regards are towards 30 nm chromatin fibers reconstructions [59], far from the analysis of single point variation or chemical alteration in a single helix of DNA.

3. – SHS for DNA imaging and characterization

3˙1. *SHS for biomolecules: working principle.* – A droplet on a hydrophobic surface, due to a peculiar combination of liquid/solid/air interfaces, can assume several shapes (such as flat, hemisphere or spherical) on the basis of the surface tension, without spreading. In the case of super-hydrophobicity, the droplet assumes a quasi-spherical shape showing a contact angle with the surface greater than 150° [60]. This phenomenon is spontaneously occurring in nature on some plant leaves (the so-called "lotus effect") and on several insects wings [60-62].

Super-hydrophobicity of rough surfaces has been explained by the Wenzel or Cassie states. In the Wenzel state, the solution droplet adheres to the solid surface, showing large contact and rolling angles [63]; in the Cassie state the solution is only in partial contact with the solid and the droplet has large contact angles while the rolling angles are small [64, 65] (fig. 8).

This characteristic has stimulated researchers to design super-hydrophobic devices mimicking what happens in nature. A variety of patterned surfaces and related tech-

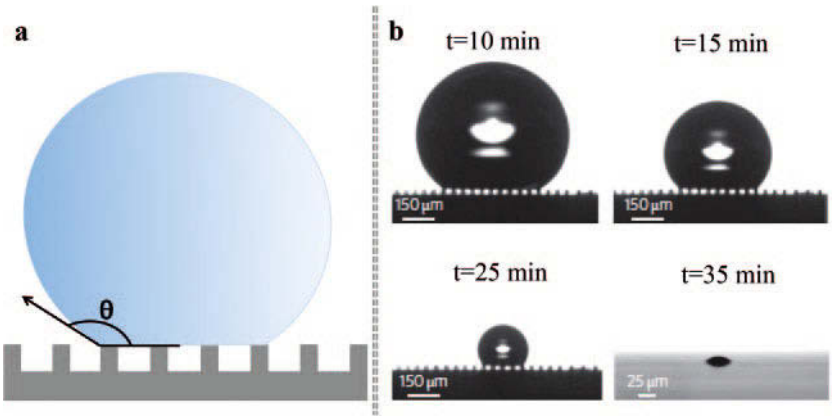

Fig. 8. – Evaporation of a droplet on a super-hydrophobic surface. (a) Model showing the high contact angle and the drop deposited on a substrate; the solution is not in contact with the lower part of the surface of the substrate during the dewetting process. (b) Microscopy image of a vertical section of a solution droplet before and after evaporation, pointing out the droplet sliding. Readapted with permission from [66].

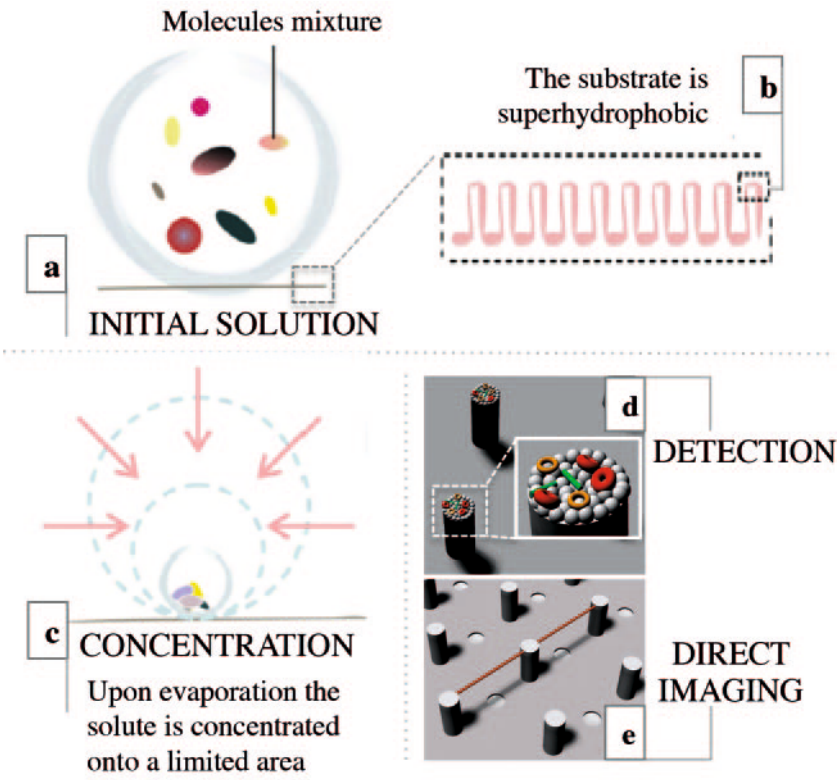

Fig. 9. – Sketch of the device working principle. (a) A droplet of solution containing a diluted molecules mixture is deposited on (b) the micro-patterned super-hydrophobic substrate. (c) The de-wetting process (diffusion/convection/evaporation) causes the reduction of droplets' volume while keeping its semi-spherical shape. In the meanwhile, the material contained in the solution is precipitated and concentrated into a defined area. Readapted from [74]. (d) The mixture of molecules can be deposited on the top of functionalized pillars, allowing the detection of diluted materials. (e) The droplet slides from one pillar to another during the evaporation process and, with this natural movement drags the molecules previously linked to the top of the pillars.

niques have been developed for the most different applications [67], including industrial applications, self-cleaning surfaces, high-throughput lab-on a chip processes [68], microfluidics [69], membranes for water purification [70], separation of oil from water and the biological characterization of diluted solutions [66, 71-73]. A low amount of biopolymers such as protein or DNA can be efficiently deposited on periodical arrays of micropillars, offering promising routes to sensing technologies [71] and novel high resolution imaging techniques [73].

In this review, the roughness ensuring a high contact angle is given by ordered arrays of micro-pillars (fig. 9). Different patterns and materials of super-hydrophobic devices were micro-fabricated in our group, on the basis of the downstream application; in all cases reported, the high contact angle and low friction coefficient are maintained and the suspension of materials between the micro-asperities of the substrate (fig. 9d, e) is obtained.

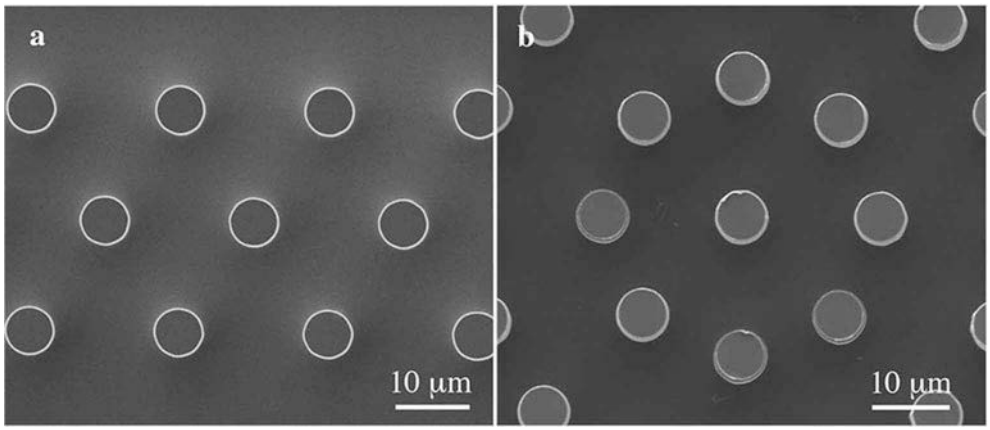

Fig. 10. – Super-hydrophobic devices. Silicon-based micro-fabricated devices showing a top view of the (a) hexagonal and (b) circular patterns widely used and characterized in our works.

Several examples of the use of super-hydrophobic devices are reported in the bibliography but the novelty in our approach is to combine the super-hydrophobic phenomena with the suspension of long DNA fibers (several microns) with nanometric diameter in order to achieve background-free TEM imaging. The technique is successful also with DNA interacted with protein and cell membranes, but the results are not included in this review.

The patterns of the super-hydrophobic surfaces (SHS) herein used, comprise micro-fabricated cylindrical pillars with a precise diameter and pitch to guarantee with high stability the hydrophobicity of the device. Two of the favored geometries proposed are hexagonal (fig. 10a) and circular (fig. 10b), even if more complex designs in which the periodicity is broken have been reported [75]. Micro-pillars were fabricated by using materials such as SU8 [76], PMMA [77, 78] or silicon [66, 73, 79] by combining different techniques such as laser writer, optical lithography and reactive ion etching (details of the fabrication processes are reported elsewhere [80]). In some cases, the top of the silicon-based micro-pillars were modified to incorporate nanoporous silicon-films (NPSi) [81] or silver nanostructures [82, 83]. A thin layer of teflon-like polymer or perfluorodecyltrichlorosilane (FDTS) was deposited at the end of the process to provide contact angles higher than 160°; the thickness of this layer was investigated by atomic force microscopy. The results of the micro-fabrication were verified by scanning electron microscopy (SEM) as for the experimental results with biomolecules.

3˙2. *DNA direct imaging.* – When a molecule dissolved in the buffer solution is long enough to cover the pillar-pillar distance (gap), it is possible to observe a distinct deposition mechanism: as long as the evaporation proceeds, deposition and suspension of DNA molecules between pillars takes place (see fig. 9e). Herein we will focus on the suspension of nucleic acid molecules over the SHS and on their structural characterization with high-resolution imaging and spectroscopic techniques.

Lambda DNA (λ-DNA) is a double-strand nucleic acid isolated from the bacteriophage lambda (cI857*ind* 1 *Sam* 7) and its sequence of 48502 base pairs in length has been widely characterized since the '80s [84, 85]. The length of the DNA strands corresponds approximately to 14.5 μm considering its B-form and 13.1 μm if considering the A-form;

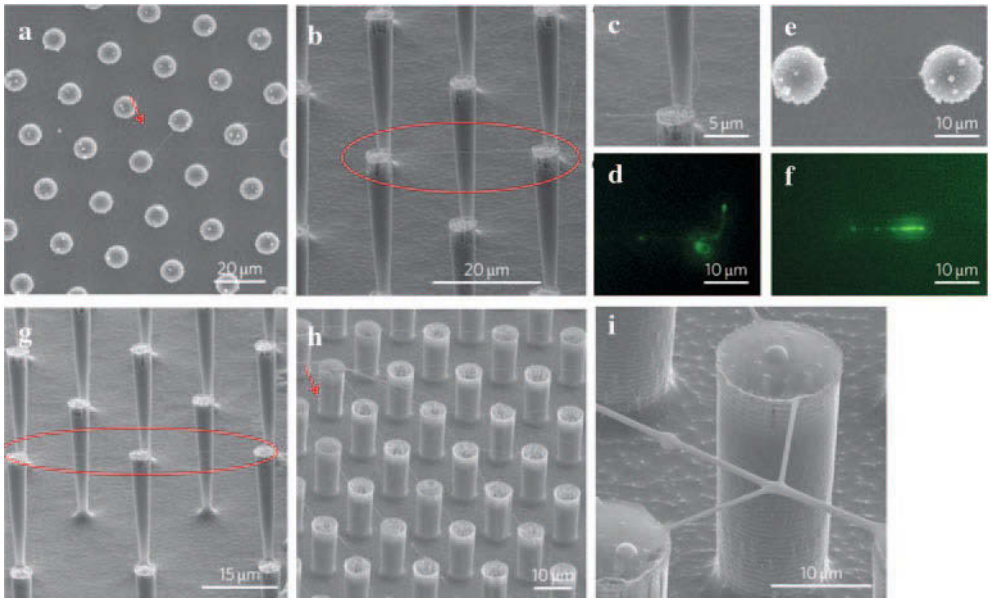

Fig. 11. – SEM images of λ-DNA suspended between micro-pillars arranged in a hexagonal pattern. In (c)-(f) SEM micrographs with correspondent fluorescent images are taken by using an optical microscope. Reprinted with permission from [66].

both these calculated measures distances can cover the pillars' gap of 12 μm. λ-DNA has been chosen then as a suitable test system due to its length, and the high reproducible sample preparation.

In a first approach reported in [66], we have demonstrated that nucleic acids can be suspended over a hexagonal pattern of cylindrical micro-pillars. The titration performed using a phosphate buffer solution allowed the researchers to obtain DNA filament of 15 to 30 μm in length, as shown by the SEM images reported in fig. 11. The method was further verified by fluorescence microscopy; an attomolar concentration of dsDNA was incubated with a fluorescent stain (YOYO-1) commonly used as a nucleic acids bis-intercalator. The different diameters of the fibers and the lengths covered by the dsDNA suspension, suggested that several nucleic acid double helices were overlapping in almost the same position, originating the bundles shown in fig. 11.

The ability to control the deposition of DNA molecules on silicon micro-patterned devices has been further improved in [79] by adjustments of the deposition process and of the device properties.

The latest SHS are constituted by silicon micro-pillars and holes passing throughout the device, conveniently aligned between the micro-structures. This device architecture allows its use in a TEM instead of the common grids. The microscope electron beam illuminates the SHS and hits the bundles suspended over the holes, as shown in the sketch of fig. 12.

The SHS are constituted by silicon-based micro-pillars arranged to form a regular hexagonal pattern; the devices incorporate also the above-mentioned pattern of circular holes (fig. 13). A thin layer of Teflon-like polymer (estimated to be around 2 nm) was finally deposited all over the surface to guarantee the device super-hydrophobicity.

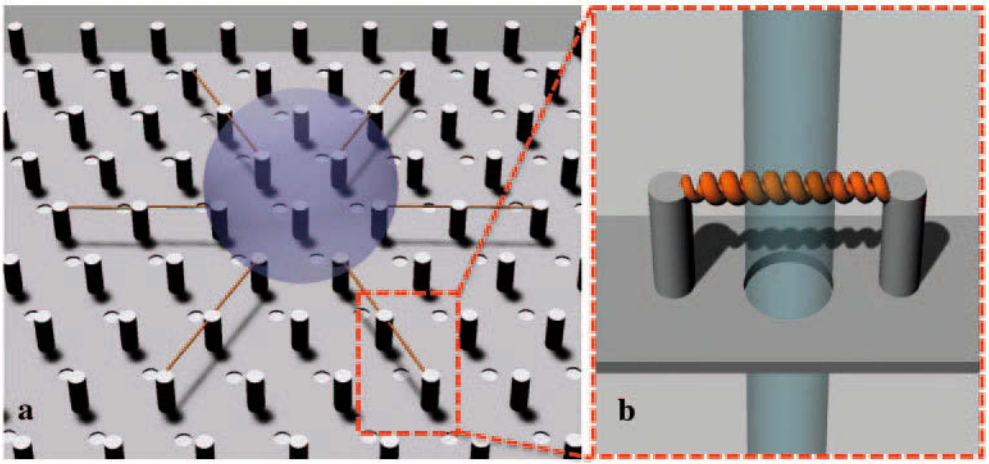

Fig. 12. – (a) The modified SHS device has holes between micro-pillars. This allows the direct imaging of the material suspended between micro-pillars when (b) the beam passes through the hole.

λ-DNA was diluted to a final concentration of 50 ng/μl in a phosphate buffer solution (PBS) containing an optimized amount of monovalent cation (0.137 M NaCl); a 20 μl of the freshly prepared solution was deposited over SHS. The dehydration occurred overnight in a closed Petri dish at a temperature of 24 °C and 50% of humidity. The results of the dewetting were preliminarily characterized by SEM (fig. 14) and the device

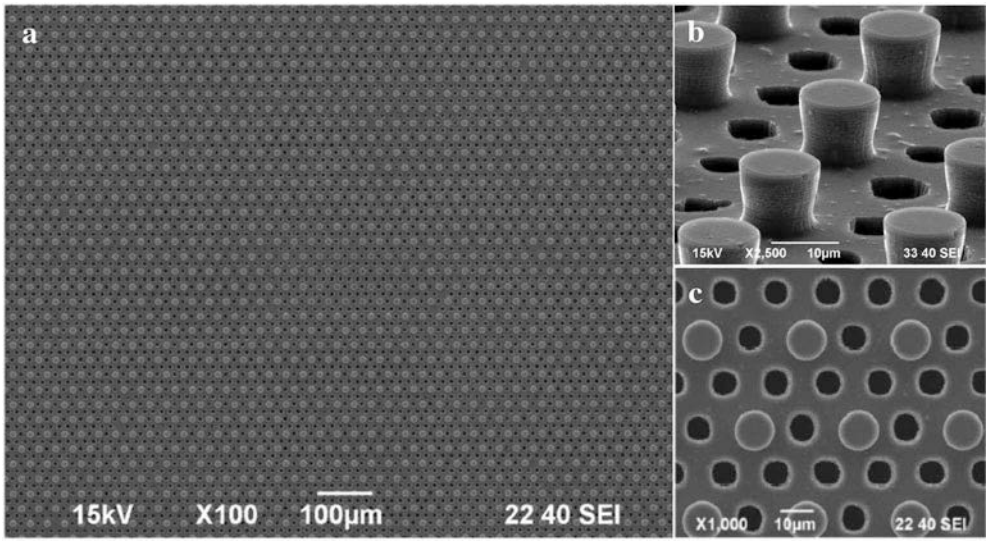

Fig. 13. – SHS with silicon micro-pillars arranged into a hexagonal pattern were modified with a pattern of holes between pillars at different magnifications. The presence of the holes allows the electron beam to impact on the suspended sample. Reprinted with permission from [86]. Material under CC BY 3.0.

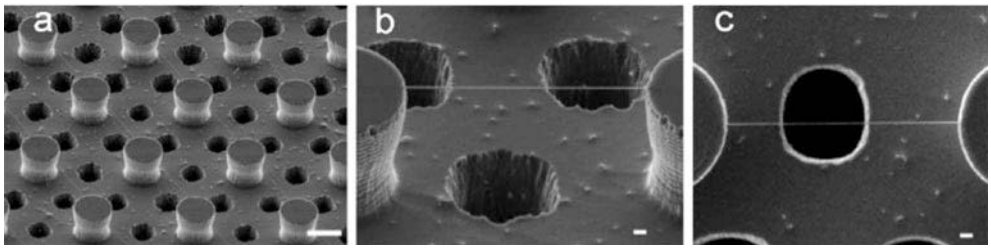

Fig. 14. – (a-c) SEM images of suspended DNA bundles over SHS. Scale bar in panel (a) = 10 μm; in panels (b), (c) = 1 μm.

was then loaded in a TEM. The DNA fibers suspended between micro-pillars and located over the holes can be directly imaged by the TEM electron beam, which can freely pass through the discontinuities of the device. A bundle of 8 nm diameter has been imaged, operating at an acceleration voltage of 100 keV, revealing the period of the DNA in the A-form (fig. 15). Ten periods of dsDNA are shown in the inset of fig. 15a; each period is reported in the histogram and measures 2.7 ± 0.2 nm, in good agreement with the data previously reported for the X-ray diffraction of A-DNA fibers [8].

To further confirm these results, the fast Fourier transform (FFT) was analyzed: a clear maximum is observed at 0.37 ± 0.02 1/nm, corresponding to the frequency of 2.7 ± 0.2 nm (fig. 15d).

The model we provided for the 80 Å bundle is an arrangement of $6 + 1$ double helices, with one central helix surrounded by other 6 helices (see fig. 16). The total diameter proposed in the simulation is around 80 Å, considering spacing between the helices due to the hydration state of the molecule. We assume that, in our working conditions, the

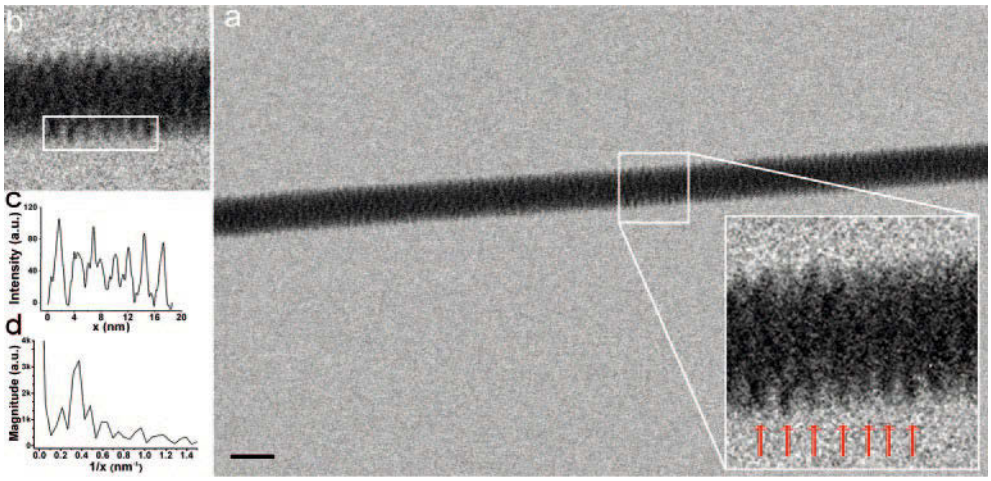

Fig. 15. – (a-b) TEM image with intensity profile of a 80 Å λ-DNA bundle. The inset in panel (a) shows 10 periods of A-DNA; the red arrows highlight the 2.7 nm pitch of the helix, confirmed by the analysis of the intensity profiles reported in (c). In (d) is reported the FFT of the signal displayed in (c): the maximum observed at 0.37 ± 0.02 1/nm corresponds to a frequency of 2.7 ± 0.2 nm.

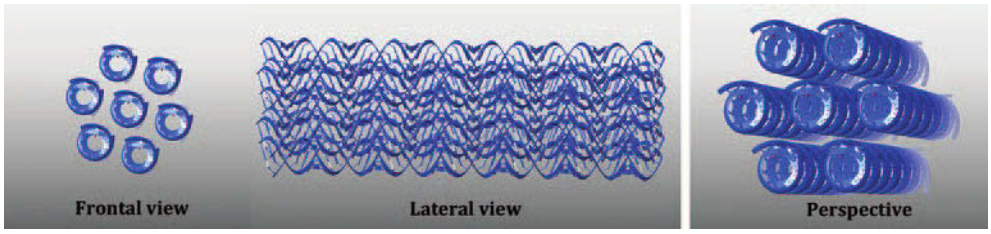

Fig. 16. – Sketch showing the $6 + 1$ helices model. A bundle of 7 helices has a diameter of approximately 80 Å. An interspacing of the helices of 2.5 Å, due to solute presence, has been taken in consideration in the simulations. The sequences used to construct the model reported in this figure are arbitrary 70 base pairs extracted from the 48502 available for the whole Lambda DNA sequence.

external relative humidity is less than 75% and the DNA inter-distances are expected to be approximately of 2.5 Å.

The cylindrical micro-pillars used in the work of Gentile *et al.* [79] had a height h of about 12 μm, a diameter d of 10 μm and a pitch δ of 30 μm. The distance between micro-pillars on the patterned SH device is a critical parameter due to the limitations given by the nucleic acids length. In a later work of Marini *et al.* of 2015 [73], the SHS device was further modified and the DNA solution preparation step was tuned and improved. The imaging process has been successfully optimized and performed to reach the single-base resolution.

The SHS was re-designed and a circular pattern of cylindrical silicon micro-pillars was newly introduced, still mantaining the round-shaped holes between the micro-pillars. To maintain the desired super-hydrophobicity of the device, the diameter of the micro-pillars was reduced to 6 μm while the height was kept of approximately 12 μm. As previously reported, a thin layer of a Teflon-like polymer has been deposited on the device prior to use (fig. 17). This geometry has been extensively tested and titrated with respect of

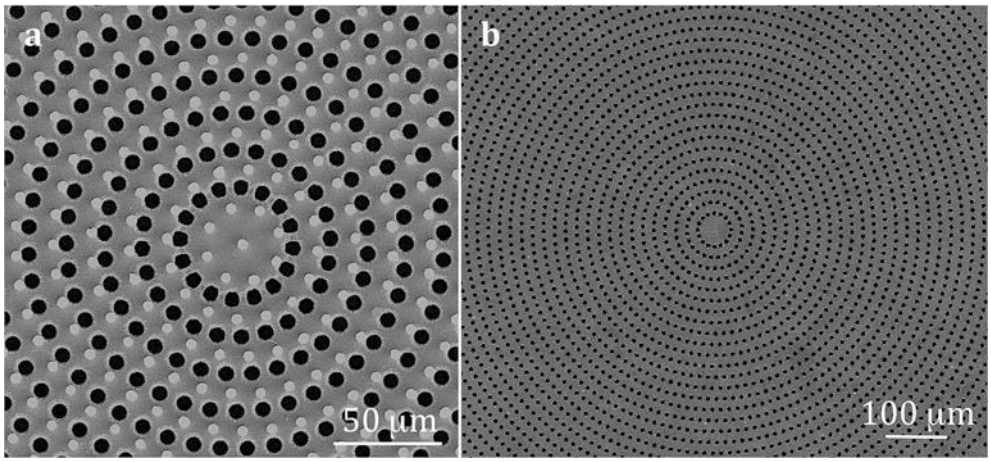

Fig. 17. – Optimized SHS for single-molecule imaging of dsDNA. (a) Silicon micro-pillars were arranged in a circular pattern. (b) On the other side of the device only the holes are visible.

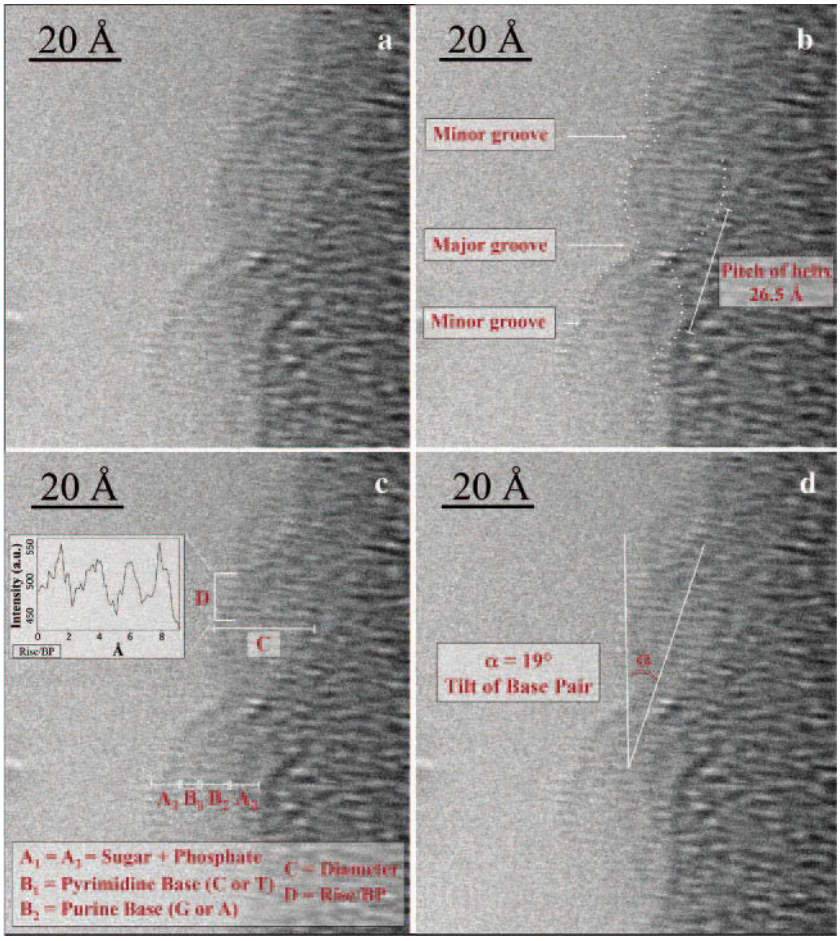

Fig. 18. – A-DNA direct image acquired by HRTEM and related metrology. (a) HRTEM phase-contrast image of a single A-DNA helix bound to a 100 Å DNA bundle obtained by stacking of two images. (b) Major and minor grooves and the helix pitch of 26.5 Å are highlighted by the dotted line. (c) Backbone, bases, diameter, rise per base pair are indicated. Notice that the lengths of two different base pairs are shown. (d) The tilt of the base pairs with respect to the helix axis is of 19°. Reprinted with permission from [73] © 2015, The Authors.

other geometries, showing the best results in the sliding of the droplet towards the center, the dewetting process and the single-molecule extension between micro-structures (data not shown).

An optimized solution of λ-DNA was used. A buffer saline solution compatible with physiological conditions was titrated spanning a range of *p*H from 7.0 to 9.3. A range of concentrations (5 to 10 mM) of the monovalent cation (Na^+) was tested too, evaluating a 0.5 mM steps. The parameters that allowed the best results saw the use of a 6.5 mM NaCl, 10 mM Tris-HCl *p*H 9.3 saline buffer solution. λ-DNA was diluted in the mentioned buffer at the final concentration of 50 ng/μl and a droplet volume of 5 μl was then deposited on the SHS. The imaging has been performed using a Titan 60-300 electron microscope (FEI) equipped with a high-brightness electron gun (x-FEG), a Wientype monochromator, a spherical aberration (Cs) corrector of the objective lens and a Tridiem 865 Gatan image

TABLE II. – *A-DNA lengths. The lengths measured from fig. 18 are reported in column* 2. *The statistical error for the measured lengths is estimated to be* 1.5 Å *from the inset of fig.* 18*c. In column* 3 *the correspondent accepted values from X-ray data* (‡) *and simulations* (†)*, in good agreement with our measurements. Notice that five new structural features were directly measured. Reprinted with permission from* [73]. © 2015*, The Authors.*

A-DNA structural characteristics	HRTEM measurements (Å)	X-ray and simulation data (Å)
Diameter	21.2	$23.0^{\dagger}$
Rise/base pair along axis	2.5	$2.6^{\dagger}$
Pitch/tum of helix	26.5	$28.2^{\dagger}$
Phosphate + sugar (backbone A_1)	5.1	$5.3^{\ddagger}$
Base (B_1)	3.6	$4.0^{\ddagger}$
Base (B_2)	5.2	$5.4^{\ddagger}$
Phosphate + sugar (backbone A_2)	5.0	$5.3^{\ddagger}$
Base length ($B_1 + B_2 +$ base interdistance)	11.3	$11.5^{\ddagger}$
Tilt of base pair relative to the axis	19°	$19^{\circ\ddagger}$

filter (GIF) coupled with an UltraScan 1000 2K × 2K charge-coupled device camera. The microscope was operating at electron beam energy of 80 keV and the magnification used was of 1 million. Among the different tensions available and tested (300 keV, 200 keV, 120 keV), the 80 keV acceleration voltage has been chosen as the best compromise.

The HRTEM image obtained of a single double helix and the related metrology are shown in fig. 18. In panel (a) a stack of two images is reported, showing the A-DNA double helix bound to a 100 Å DNA bundle. The detailed metrology is reported in panels (b) to (d). The "macroscopic" features of DNA such as the diameter of 20 Å, the period and the bases tilt with respect to the axis (19°) are easily measurable and both the major and the minor grooves are visible (lengths are highlighted by the dotted line of panels (b) and (d)). The calculated resolution was of 1.5 Å [87] and the contrast achieved with this preparation method allowed us to directly quantify not only the well-known features such as the inter-base pair distance, pitch and diameter but also the backbone and the bases lengths (panel (c)). The backbone, indicated with A_1 and A_2, has a length of ~ 5 Å and corresponds to the simulated phosphate + sugar. Our study revealed a phosphate backbone of 5 Å (A_1 and A_2 in fig. 18(c)), in good agreement with the simulated data. The pyrimidine base B_1 has a length of 3.6 Å and the purine B_2 measures 5.2 Å [14, 88]. The measures herein reported are in good agreement with the simulated data. In our knowledge this is the first time that the bases were directly visualized and measured. The detailed measures achieved are summarized in table II. Notice that, if compared to the accepted X-Ray values (column 2), five new molecular features were measured, previously available only upon modeling.

HRTEM images obtained at different Na^+ concentrations and operating at different voltages are reported in fig. 19. The titration of the salts dissolved in the buffer solution had the fundamental role to obtain thinner bundles and to expose one DNA double

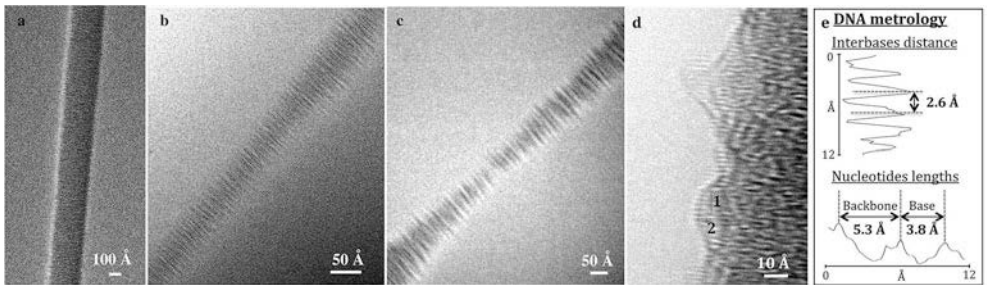

Fig. 19. – HRTEM images of DNA. (a-c) Different concentrations and different voltage were used to achieve (d) the single-molecule resolution. In panel (e) is reported the metrology of the dsDNA helix exposed to beam in panel (d): the interbase distance and nucleotides lengths were directly measurable due to the improvements in contrast and resolution.

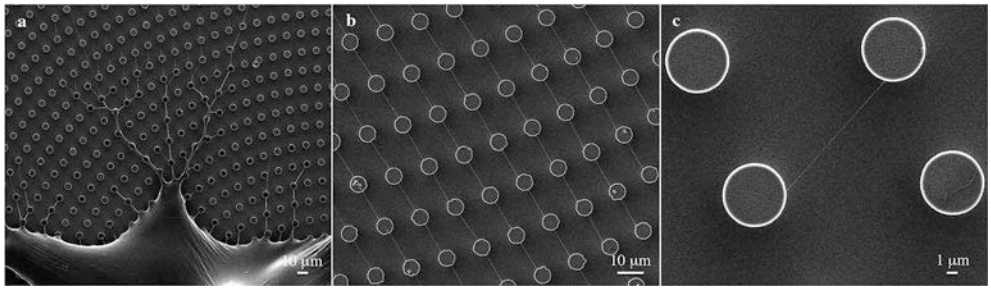

Fig. 20. – Circular pattern of cylindrical micro-pillars with human genomic DNA suspended over a wide macro area of the device.

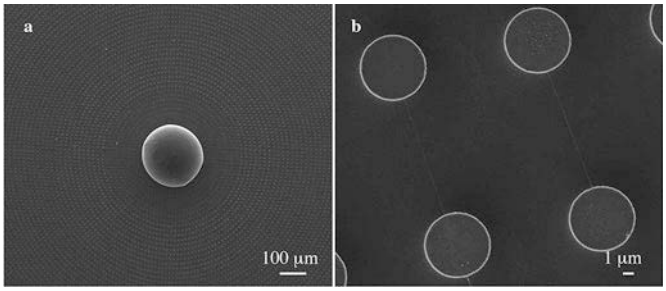

Fig. 21. – ssDNA molecules deposited on a circular micro-patterned device. The behavior is analogous to the one reported for dsDNA, confirming the versatility of the device. (a) The saline buffer removed from the bundles is confined in an area of approximately 200 nm and (b) an example of two ssDNA bundles covering the micro-pillars distance of 12 μm.

helix to the electron beam. In fig. 19c a low magnification micrograph shows a region of less than 50 Å diameter. In fig. 19d is reported a HRTEM image showing further improvements in the contrast and resolution of the fine details of the double helix [89]; the interbases distance is of 2.6 Å and it is in good agreement with the metrology obtained from fig. 18. The backbone and the base lengths were clearly visible and measurable (5.3 Å and 3.8 Å, respectively, fig. 19e) without any need of image stacking.

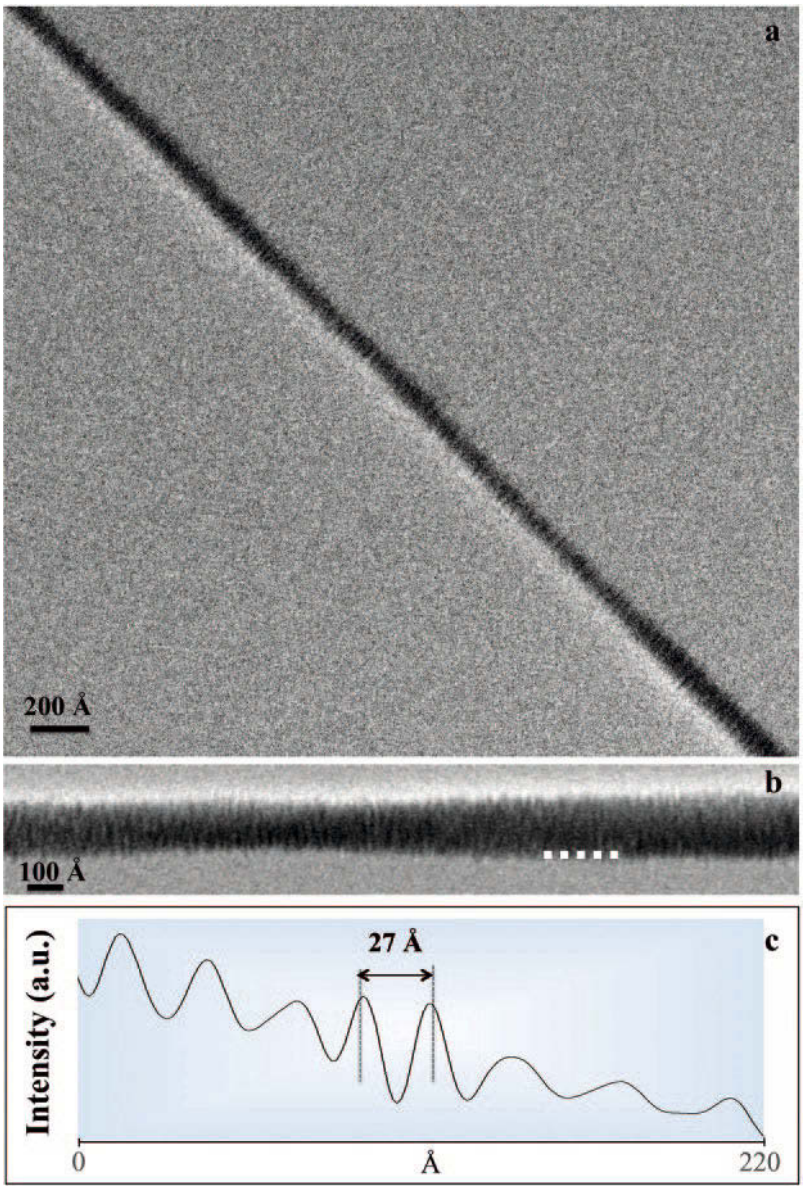

Fig. 22. – TEM images of ssDNA (a-b) and related metrology (c), showing a period of 27 Å. Both images were taken working at an acceleration voltage of 100 keV.

Recently, human genomic dsDNA has been preliminary used by our group on a circular pattern of cylindrical micro-pillars [90]. The length of this kind of dsDNA has been tested by pulsed field gel electrophoresis (PFGE) and, at the moment of writing, the solution obtained is composed by a plethora of fragments longer than 50 kb. Despite the non-homogenous size of the starting solution, the suspension over SHS is promising: the bundles obtained by using human genomic DNA at concentration ranging between 60 pM and 1 pM are shown in fig. 20.

Single-strand DNA of calf thymus has been already tested on the devices, showing promising results for the single-molecule suspension between micro-pillars [91]. The results of the dehydration process are in good agreement with what reported previously for the double-strand helices of the λ-DNA and the genomic DNA samples; ordered fibers of DNA are suspended between micro-pillars over a macroarea of hundreds of microns, confirming the versatility of the device. The diameter of the bundles measured ranges between 150 nm to 5.5 nm, suggesting that bundles made of several DNA strands shells down to only three helices were suspended on the device (fig. 21).

ssDNA from calf thymus of approximately 50 kb was also tested for TEM imaging. The DNA periodicity of 27 Å has been measured by the intensity profile reported in fig. 22.

3˙3. *Micro-Raman and SERS characterization of nucleic acids.* – The information achieved by direct imaging on nucleic acids bundles has been integrated with spectroscopic measurements. As previously reported, Raman (fig. 23) and SERS techniques can be successfully applied to biological materials deposited on properly micro-structured devices. Several attempts to investigate the structural characteristics of biological molecules were performed in our group [72,91]. The comparative study between dsDNA and ssDNA revealed spectral differences within the range 500-1900 cm^{-1} (fig. 23a). Besides the characteristic bands related to the deoxyribose sugar, bases and backbone which are common for both the nucleic acids, some differences were also identified. The peaks centered at around 931, 985, 1298 cm^{-1} and the peak shift from 1132 to 1141 cm^{-1} can be related to the hydrogen bonds occurring between complementary bases in the double-strand conformation of the nucleic acid.

In addition, an optical image of suspended ssDNA and the overlapping 2-D mapping analysis centered at 2960 cm^{-1} are reported in fig. 23b. A Raman spectrum of ssDNA in the region 2500-3500 cm^{-1} shows characteristic bands centered at around 2900 and 2960 cm^{-1}, associated respectively to the symmetric C-H_x stretching (aliphatic) and the asymmetric C-H_x stretching (aromatic) vibrations.

In a later work [91] we were able to demonstrate that the combination between SHS, optimized biological preparation and non-destructive Raman spectroscopy allows the assignment of the conformational status of the suspended helices, in other words the

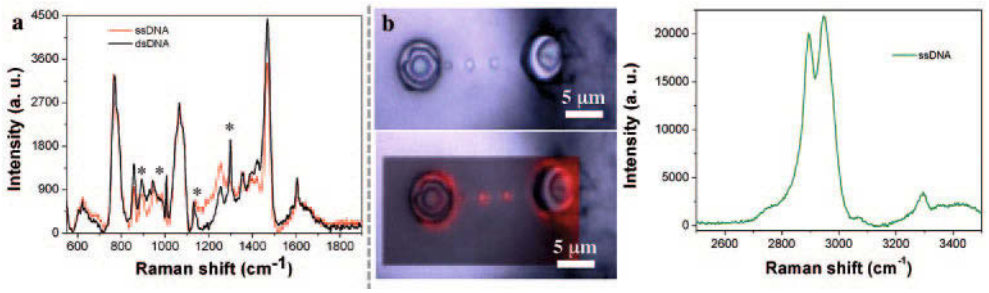

Fig. 23. – (a) Raman fingerprints of ssDNA and dsDNA obtained by single-scan measurements on suspended DNA fibers. The asterisks highlight the differences between the two nucleic acids. (b) Optical image of ssDNAs suspended over a SHS and (c) superimposed 2-D mapping analysis for the Raman band centered at 2960 cm^{-1}. (d) Typical Raman spectrum of ssDNA in the spectral range of 2500–3500 cm^{-1}. Readapted from [72].

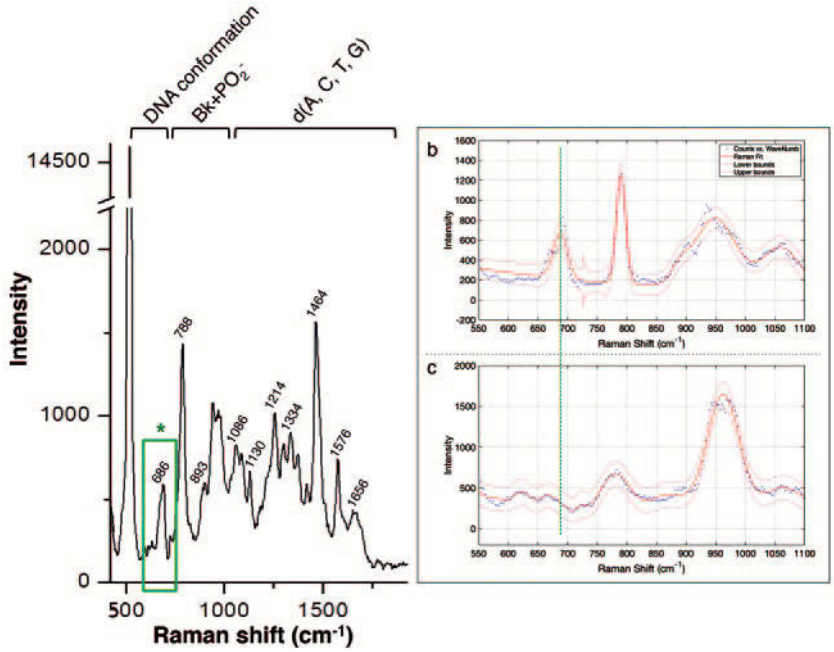

Fig. 24. – Raman spectra of a dsDNA suspended bundle. (a) Several DNA's characteristic bands were assigned. The region 600-700 cm^{-1} of two distinct spectra regarding the (b) B-form and the (c) A-form has been analysed; the Raman fits show bands centred at 688 cm^{-1} and 670 cm^{-1}. Published with permission from [91] © 2017 Elsevier B.V. All rights reserved.

hydration of the investigated bundle. DNA prominent bands were assigned, as shown in fig. 24. Over the spectral range considered (450-1800 cm^{-1}), the region 600-700 cm^{-1} has been selected as the one sensitive to conformational changes in the double helix. The Raman fits of two distinct single-scan measurements reported in fig. 24b, c showed separate bands centred at 688 cm^{-1} (B-DNA) and 670 cm^{-1} (A-DNA) [92-94]. These data showed that bundles have a strong B-DNA component, even if the HRTEM imaging points out a precise A-DNA. We strongly believe that the metrology achieved up to now has to be referred only to the dehydrated outer helices of the bundles, while the inner helices maintain a hydration shell, sufficient to confer to the molecule its B-form.

4. – SHS technology for different applications

The micro-structured surfaces were used not only to image and characterize nucleic acid molecules but also for several other tasks such as concentration of highly diluted solutions, localization, detection and related spectroscopic studies, cells seeding and for micro crystals growth.

Herein we report about the investigation of molecules such as the dye rhodamine 6G (R6G), spanning then to molecules with a major role in biology as proteins (BSA, lysozyme, amyloid fibers), exosomes and, finally, to neurons growth.

4˙1. *Molecular concentrator: few molecules detection and characterization.* – The detection of few/single molecules is of extreme interest in several fields. Just to mention

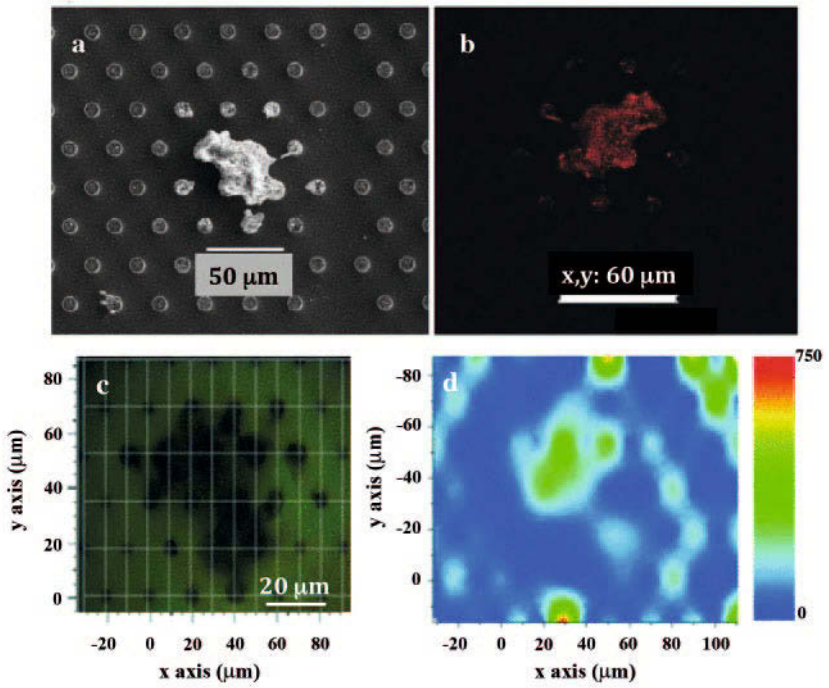

Fig. 25. – (a) SEM image of a Rhodamine 6G agglomerate obtained by a droplet dehydration containing an initial 10^{-18} M concentration of the analyte and (b) confocal fluorescent image of the same object. In (c) optical image of the device and (d) corresponding Raman mapping. Published with permission from [95] © 2013, Springer Science+Business Media Dordrecht.

some, diseases early detection and diagnosis is of fundamental importance in cancer therapy or in pathologies in which the prompt patients' treatment enhances the possibility of a successful recovery. Further, environmental pollution and safety have to be taken in consideration for human health as well: harmful gases, volatile organic compound, heavy metals even if present at low concentration can be a concern when the uptake occurs even at low concentrations. In these examples the development of devices with plasmonic properties can be considered a useful tool to extract a stronger spectroscopic signal, in order to determine the presence or absence of low amounts of diluted molecules [96, 97].

Several attempts to develop detection platforms have been made from our group. The capability of the SHS to concentrate solutions has been exploited in this context to investigate an highly diluted solution of Rhodamine 6G (R6G) [74, 83, 98]. Superhydrophobic devices constituted by a hexagonal lattice of cylindrical micro-pillars were designed, including silver nanoparticles aggregates on top of the pillars. This adaptation has the purpose to introduce SERS properties into the device, allowing increasing the Raman signal of a molecule adsorbed on pillars top.

With this method, a concentration of 10^{-18} M of R6G diluted in water was drop-casted on the device and the results of the evaporation were imaged by SEM and fluorescence microscope (fig. 25a, b). The residual of the dewetting process is, as expected, confined to a well-defined area, in this case of approximately 60 μm of diameter, starting from an initial footprint of about 2 mm.

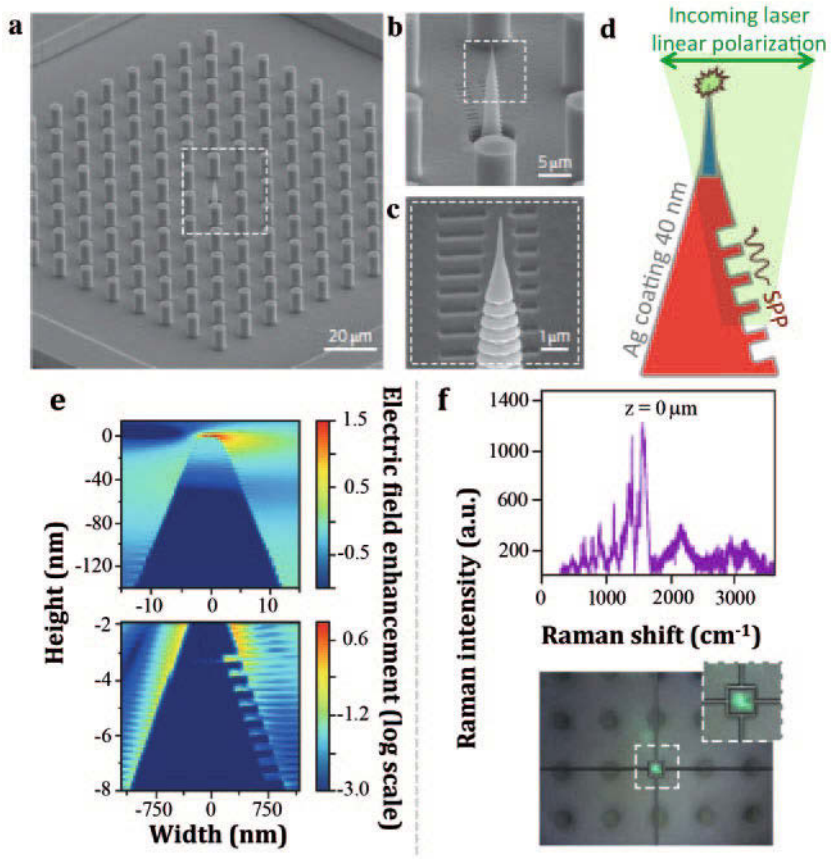

Fig. 26. – (a-c) SHS device with a plasmonic nanocone embedded in a hexagonal pattern of cylindrical micro-pillars. (d) After the complete evaporation of the droplet, the solute is concentrated on top of the nanostructure. (e) FDTD simulation results and (f) Raman measurements on lysozyme molecules in correspondence of the cone apex. Readapted from [66]. © 2011, Rights Managed by Nature Publishing Group.

The Raman mapping measurement that followed the evaporation confirmed the presence of the molecule object of investigation; the analysis of the peak centered at $1650\,\mathrm{cm}^{-1}$ showed a clear correspondence between the R6G agglomerates on the SHS and the Raman signal acquired (fig. 25c, d).

As previously reported from the same group [99], also plasmonic microstructures such as antennas or plasmonic tips can be useful tools to detetct few molecules (fig. 26). This concept, combined with the super-hydrophobic devices, leads to the design of a novel surface constituted by ordered silicon micro-pillars arrays surrounding a plasmonic silver cone conveniently located in the center of the device. The droplet deposited on such a device, drove the molecules dispersed in solution directly on the central cone tip, corresponding to the final evaporation point. The grating, fabricated on the lateral side of the silver cone was designed to drive surface plasmon polaritons towards the tip, allowing collecting Raman fingerprints of the few molecules deposited on the cone's tip. With this method, a concentration ranging from 1 fM to 10 aM of the 14.4 kDa globular protein lysozyme has been detected.

4˙2. *SHS for exosomes characterization.* – Increasing the complexity of the molecules investigated, exosomes were deposited and analyzed on SHS and bio-photonic devices [77, 100]. Exosomes are small membrane vescicles delimited by a phospholipidic double layer, with dimensions ranging from a few tens nm to 100 nm [101] and containing different types of biomolecular cargo on the basis of the healthy status of the cell [102]. Tumoral cells produce an oncogenic load that can be delivered by exosomial activity to the other cells, enhancing metastasis formation and tumoral growth. In a preliminary approach to define the exosomes cargo as biomarkers for oncogenic activity, vescicles isolated from healthy and cancerous colon cell lines were drop-casted upon the silicon SHS devices with silver nanograins on the top of the micro-pillar. The SERS analysis of the devices after sample deposition revealed substantial vibrational differences between the two classes of exosomes derived from normal and tumoral lines, related to the differences in the materials they carry out from cells in the two separate cases. Exosomes derived from healthy cells showed intense peaks corresponding to lipids vibration while the vesicles belonging to tumoral cells showed high RNA content [100].

Exosomes were investigated also by Small and Wide Angle X-Ray Scattering techniques (SAXS/WAXS) [77, 78]. As previously reported, a residue remains suspended on the micro-pillars at the final point of the droplet dehydration. In the case herein reported micro-fabricated poly (methyl methacrylate) (PMMA) super-hydrophobic surfaces allowed the formation of a solid aggregate of exosomes particles, afterwards removed from the SHS and glued to a glass capillary for the downstream X-ray analysis (fig. 27). The

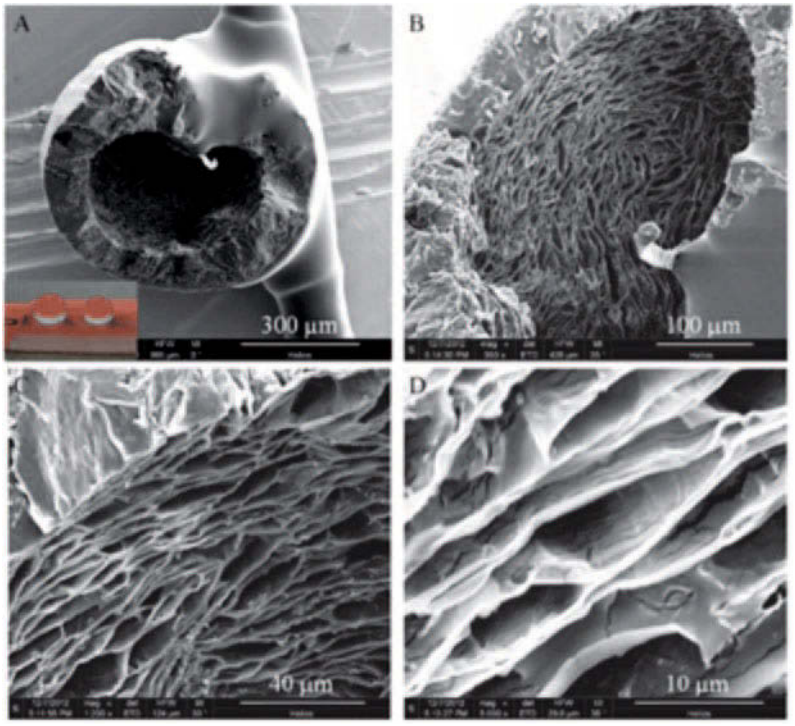

Fig. 27. – (a, b) SEM images of solid aggregates of exosome isolated from a tumoral cell line, glued to a glass capillary. In the inset two droplets deposited over a PMMA SHS. (c, d) Higher magnification SEM images of the exosome cross-cut residue reported in (a).

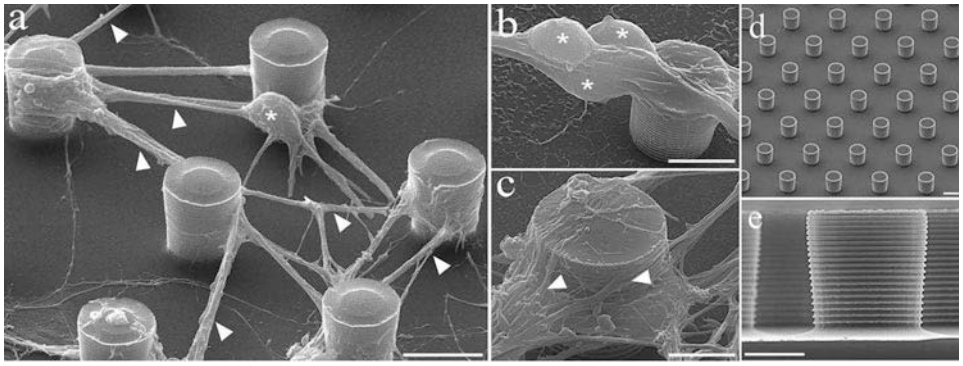

Fig. 28. – SEM images of hippocampal neurons grown on nanopatterned micro-pillars. (a-b) 3-D suspended network of neuronal somas (asterisks) and related processes (arrows). In (c) detail of the neuronal projection firmly grabbing the pillars. (d) Low and (e) high magnification images of the devices used for cells seeding. Pillars' walls were decorated with nanogrooves (height of 500 nm) to mimic the natural growth conditions of the cells. Reprinted with permission from [110], © 2013 Wiley-VCH Verlag GmbH & Co. KGaA, Weinheim.

WAXS patterns of the crystalline exosomial residue exhibited an ordered lamellar structure, in accordance with SEM imaging. The lamellar architecture is caused by the convective fluxes of the droplet while sliding and dewetting over the super-hydrophobic device. MicroSAXS patterns highlighted a more regular organization of the exosomes isolated from tumoral cells if compared to the higher disorder degree of the exosomes of healthy cell lines. This slight difference observed has been ascribed to the distance between hydrophilic and hydrophobic layers in which the membranes are naturally organized.

Similar approaches were applied to the study of lysozyme, a 14.4 kDa globular protein known to be part of hen eggs white and able to convert its alpha helices in β-sheets upon pH change. This interchange mechanism and the amyloid fibrillation are not completely understood but is widely known their relation with several neurodegenerative diseases such as Parkinson and Alzheimer diseases [103,104], prion diseases [105], amyloidosis [106, 107], etc. In [108], a weakly acid lysozyme solution in a high ionic strength condition has been deposited on micro-structured PMMA devices. Under these conditions, the formation of a fibrillar amyloidic deposit and the cross β-sheets structure formation occurs [109] and has been observed to occur at a higher rate than the one reported in the literature. Ultra-small aliphatic peptides that self-assemble into cross-β-type fibers have been recently analyzed by means of different techniques such as electron microscopy, circular dichroism, X-ray diffraction and supported by molecular dynamics simulations [107].

4˙3. *SHS and neurons growth.* – The micro-fabricated silicon-based pillars herein proposed can undergo modifications of their surfaces to mimic the cellular and extracellular complex features responsible for cellular division, motion and development [110]. In order to favor neurons' growth, a hexagonal lattice of micro-pillar was provided of a regular pattern of nanogrooves on their walls to yield a spatial modulation in the z-direction and the device was then used for cells seeding. SEM was performed to monitor cell growth and their interaction with the microstructures (fig. 28): a suspended 3-D network of cells with their projection grabbing pillars' groove has been imaged. Further, the viability assays performed on the neurons grown on the devices, showed a lower mortality than the ones grown on standard culture dishes.

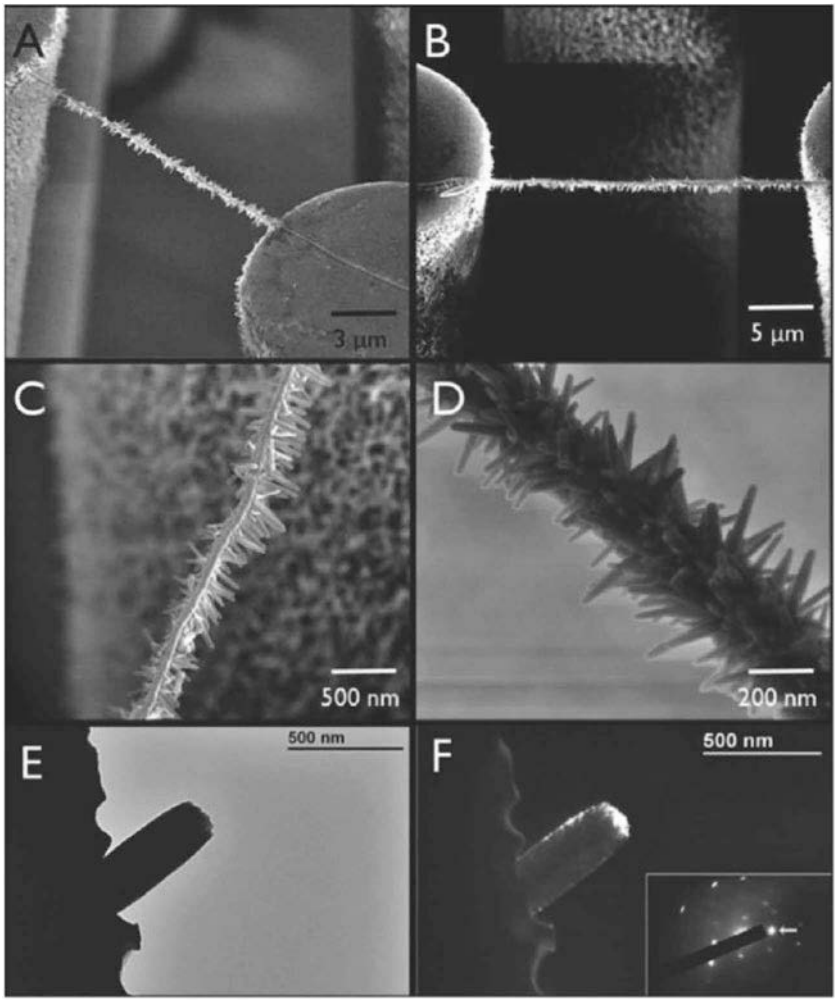

Fig. 29. – (a–d) SEM images of DNA bundles coated with gold and radially decorated with ZnO crystals. (e) Bright field TEM image of a ZnO crystal and (f) corresponding dark field image, confirming the hexagonal crystalline structure of ZnO. Reprinted with permission from [76], © 2013 Wiley-VCH Verlag GmbH & Co. KGaA, Weinheim.

The combination of the results highlights that the nanopatterned super-hydrophobic surfaces are a convenient tool for primary hippocampal neurons differentiation and that they allow the formation of viable and functional neuronal networks, a feature exploited in the development of biocompatible and biodegradable devices [111].

4˙4. *DNA as a scaffold*. – As previously mentioned, DNA suspended over super-hydrophobic devices resembles a network, autonomously organized on a regular pattern. Despite their content in genetic information, DNA bundles can efficiently be used as scaffolds and supports for other materials growth and hybridization. A first attempt to use DNA nanowires for scaffolding applications has been recently performed in [76], were λ-DNA has been deposited over a hexagonal pattern of micro-pillars. Thirty nanometers

of gold were thermally evaporated over the suspended DNA to demonstrate the viability of the bundles for conductive circuitry. The SH device, made of SU8, guaranteed the electrical isolation from the bottom layer and the electrical measurements were performed contacting individual micro-pillars with tungsten micromanipulators. Au-coated DNA nanowires were made more functional adding a radial decoration of ZnO micro-crystals (fig. 29) by hydrothermal growth. The results obtained confirmed that the device could be applied to a wide range of purposes and in this specific case to fabricate hybrid metal-organic semi-conductive wires.

5. – Drawbacks in direct imaging approach

When working with single DNA fiber or bundles with few DNA fibers, damage due to photoinduced and knock out effects is always an issue and can both limit the spatial resolution for beam-sensitive specimens [112, 113] and destroy the DNA bundle. An accurate choice of beam energy and current intensity has to be done, together with an appropriate strategy for image acquisition, such as low-dose multiple stacking.

Radiolysis on materials such as DNA can cause chemical bonds degradation and a consequent variation in the helice shape, position or its disruption under the beam. In the case of a direct image of suspended DNA, the possible damages to the double-helix covalent bonds are still under debate to improve our technique. Another practical effect that we noticed with our bundle is that in certain conditions, the electron beam of the TEM can induce a mechanical vibration that can be avoided with low dose and proper choice of the accelerating beam energy. With the advent of higher-sensitivity cameras, all these problems can be better dealt with and even solved. In any case, we are strongly working on a different strategy to improve bundle stability under TEM beams that includes mechanical aspects and charge effect in order to reach the intrinsic resolution of TEM microscopy technique.

6. – Future perspective

Super-hydrophobic devices, micro-fabrication and the proper biological preparation steps are compatible with a wide range of chemical conditions and can be combined to analyze DNA structural variation occurring upon the interaction between the bases and chemical moieties such as chemotherapeutic agents and heavy metals.

Platinum (Pt) derived agents are known to interact with nucleophile DNA molecules producing Pt-DNA adducts [114] and they are of wide interest for their clinical purposes [115]. Pt-based molecules such as cis-diamminedichloroplatinum (cis-Pt), induce the unwinding of the double helix in the site of interaction (preferentially the N7 of purines), lengthening the polynucleotide and changing its size, charge, stability. The interaction between heavy metals such as silver, platinum, chromium and the N7 of purines or N3 in pyrimidines, leads to the disruption of hydrogen bonds, with critical effects on the double-strand characteristic features [116]. Both of these alterations in the DNA native conformation perturb severely the interaction with molecular machines, inhibiting the normal cellular biological activities. High-resolution TEM imaging can be of great help on the fine-tuning in the administration of chemotherapeutic agents.

Heavy metals such as nickel, chromium, cadmium, lead, etc. are classified as carcinogens. The precise mechanism of carcinogenesis is still under debate; nevertheless, they

seem to severely interfere with different DNA repair pathways, effect ascribable to DNA morphological alterations. In this context, the elucidation of the interaction between nucleic acids and heavy metals, both for sensing and structural purposes, can be of great help in understanding their carcinogenic effects.

The present approach that combines SHS, DNA suspension technique and TEM imaging has been further extended to the imaging and characterization of DNA-protein interaction and cells membranes with promising results [89]. As a further step, with our method it will be possible to investigate molecular machines, DNA/proteins interactions such as DNA/transcription factors and proteins embedded in the membranes phospholipidic bilayers that are mostly recalcitrant to crystallization.

In the complex system such as the one of proteins/phospholipidic membranes, the biochemical and functional studies of the distribution of membrane proteins in cells are of extreme interest in basic biomedicine and in clinics [117,118] and high resolution TEM imaging would give important information about their structure and physiology.

As a preliminary result, lysozyme amyloid fibrils were successfully suspended on micro-patterned SHS, yielding single-molecule bridges, as already demonstrated with DNA. Amyloid fibers are a hallmark of many human diseases, including the previously mentioned neurodegenerative diseases. Various techniques were used to investigate their onset and structure. However, from a structural point of view, the drawback of their characterization resides in their insolubility and in the fact that the fibrils are anisotropic, such that structural imaging techniques that can complement classical fiber X-ray diffraction and solid-state NMR are needed. Using our approach we can anticipate that, by coupling suspended fibers over SHS and Raman spectroscopy, we were able not only to detect the expected [119] principal component of the secondary structure, namely the β-sheet [120], but also its anisotropic structure, thus being of aid in the elucidation not only of the main secondary structure, but also of the side chains 3D distribution along the molecule.

Further, the proposed TEM direct imaging method can be successfully combined with novel post-processing reconstruction methods [121, 122] to achieve unprecedented three-dimensional information on biological polymers.

The DNA molecule is an appealing material for a range of applications beyond structural studies. The limited diameter of 2 nm, the repeating units and the stiffness make the double helix a versatile construction material rather than a carrier of genetic information. Widely used in bottom-up and top-down constructions, nucleic acid has been applied for the development of branched DNA molecules [123], 2-D [124, 125] and 3-D [126] nano-objects and DNA-based molecular machines [127]. DNA can be than seen as a mere scaffold, on which organize other molecules or compounds of interest that have to undergo downstream analysis such as TEM or spectroscopic characterization.

Super-hydrophobic devices, previously proposed in the last years, can allow researchers to contemporarily concentrate and investigate the DNA fragments listed above, since they are small and highly diluted in the patients' plasma [128-131]. Further, the proposed devices and the related imaging methods, combined with novel post-process reconstruction methods [121], could positively affect molecular biology study of hereditary and epigenetic changes of circulating DNA coming from patient's liquid biopsies. High-resolution imaging of this wide range of free DNA could represent an effective and complementary solution in diagnosis and prognosis of cancer, inflammation or infection diseases [131-134].

REFERENCES

[1] Levene P. A. and Jacobs W. A., "Uber die Hefe-Nucleinsaure", *Eur. J. Inorg. Chem.*, **42** (1909) 2474.

[2] Levene B. Y. P. A. and S L., "Guaninedesoxypentoside from thymus nucleic acid.", *J. Biol. Chem.*, **81** (1929) 711.

[3] Avery O. T., McLeod C. and Mccarty M. D., "Studies on the chemical nature of the substance inducing transformation of pneumococcal types", *J. Exp. Med.*, **79** (1944) 137, http://www.pubmedcentral.nih.gov/articlerender.fcgi?artid=2135445&tool=pmcentrez&rendertype=abstract.

[4] Chargaff E., "Chemical specificity of nucleic acids and mechanism of their enzymatic degradation", *Experientia*, **6** (1950) 201, http://www.ncbi.nlm.nih.gov/pubmed/8174683.

[5] Wilkins M. H. F., Stokes A. R. and Wilson H. R., "Molecular structure of deoxypentose nucleic acids", *Nature*, **171** (1953) 738.

[6] Franklin R. E. and Gosling R. G., "Molecular configuration in sodium thymonucleate", *Nature*, **171** (1953) 740.

[7] Franklin R. E. and Gosling R. G., "Evidence for 2-chain helix in crystalline structure of sodium deoxyribonucleate", *Nature*, **172** (1953) 156.

[8] Franklin R. E. and Gosling R. G., "The structure of sodium thymonucleate fibres. I. The influence of water content", *Acta Crystallogr.*, **6** (1953) 673.

[9] Pauling L., Corey R. B. and Branson H. R., "The structure of proteins; two hydrogen-bonded helical configurations of the polypeptide chain", *Proc. Natl. Acad. Sci. U.S.A.*, **37** (1951) 205.

[10] Watson J. D. and Crick F. H. C., "Molecular structure of nucleic acids", *Nature*, **171** (1953) 737, http://www.nature.com/physics/looking-back/crick/%5Cnhttp://www.ncbi.nlm.nih.gov/pubmed/13054692.

[11] Kiskinova M., Marsi M., Di Fabrizio E. and Gentili M., "Synchrotron radiation scanning photoemission microscopy: instrumentation and application in surface science", *Surf. Rev. Lett.*, **6** (1999) 265.

[12] Collins M. D. and Gordon S. E., "Short-chain phosphoinositide partitioning into plasma membrane models", *Biophys. J.*, **105** (2013) 2485.

[13] Saenger W., *Principles of nucleic acids structure* (Springer) 1984.

[14] Taylor R. and Kennard O., "The molecular structures of nucleosides and nucleotides. Part 1. The influence of protonation on the geometries of nucleic acid constituents", *J. Mol. Struct.*, **78** (1982) 1.

[15] Sette M., D'Addabbo P., Kelly G., Cicconi A., Micheli E., Cacchione S., Poma A., Gargioli C., Giambra V. and Frezza D., "Evidence for a quadruplex structure in the polymorphic hs1.2 enhancer of the immunoglobulin heavy chain 3' regulatory regions and its conservation in mammals", *Biopolymers.*, **105** (2016) 768.

[16] Yu X., Li Z., Shen J., Chan M. T. V. and Wu W. K. K., "Role of microRNAs in primary central nervous system lymphomas", *Cell Prolif.*, **49** (2016) 147, http://dx.doi.org/10.1111/cpr.12243.

[17] Yu A. A., Savas T., Cabrini S., DiFabrizio E., Smith H. I. and Stellacci F., "High resolution printing of DNA feature on poly(methyl methacrylate) substrates using supramolecular nano-stamping", *J. Am. Chem. Soc.*, **127** (2005) 16774.

[18] Teo P. Y., Cheng W., Hedrick J. L. and Yang Y. Y., "Co-delivery of drugs and plasmid DNA for cancer therapy", *Adv. Drug Deliv. Rev.*, **98** (2016) 41.

[19] Goodchild J., "Therapeutic oligonucleotides", *Methods Mol. Biol.*, **764** (2011) 1.

[20] Evers M. M., Toonen L. J. A. and van Roon-Mom W. M. C., "Antisense oligonucleotides in therapy for neurodegenerative disorders", *Adv. Drug Deliv. Rev.*, **87** (2015) 90, http://www.sciencedirect.com/science/article/pii/S0169409X15000435.

[21] Parashar A., "Aptamers in Therapeutics", *J. Clin. Diagn. Res.*, **10** (2016) BE01, http://www.ncbi.nlm.nih.gov/pmc/articles/PMC4963637/.

[22] Agarwal A., Rhoades W. R., Hanout M., Soliman M. K., Sarwar S., Sadiq M. A., Sepah Y. J., Do D. V. and Nguyen Q. D., "Management of neovascular age-related macular degeneration: Current state-of-the-art care for optimizing visual outcomes and therapies in development", *Clin. Ophthalmol.*, **9** (2015) 1001.

[23] Keefe A. D., Pai S. and Ellington A., "Aptamers as therapeutics", *Nat. Rev. Drug Discov.*, **9** (2010) 537, http://dx.doi.org/10.1038/nrd3141.

[24] Lao Y. H., Phua K. K. L. and Leong K. W., "Aptamer nanomedicine for cancer therapeutics: Barriers and potential for translation", *ACS Nano*, **9** (2015) 2235.

[25] Lu H., Busch J., Jung M., Rabenhorst S., Ralla B., Kilic E., Mergemeier S., Budach N., Fendler A. and Jung K., "Diagnostic and prognostic potential of circulating cell-free genomic and mitochondrial DNA fragments in clear cell renal cell carcinoma patients", *Clin. Chim. Acta.*, **452** (2016) 109.

[26] Connolly I. D., Li Y., Gephart M. H. and Nagpal S., "The 'Liquid Biopsy': the Role of Circulating DNA and RNA in Central Nervous System Tumors", *Curr. Neurol. Neurosci. Rep.*, **16** (2016) 1.

[27] Almassalha L. M., Bauer G. M., Chandler J. E., Gladstein S., Cherkezyan L., Stypula-Cyrus Y., Weinberg S., Zhang D., Thusgaard Ruhoff P., Roy H. K., Subramanian H., Chandel N. S., Szleifer I. and Backman V., "Label-free imaging of the native, living cellular nanoarchitecture using partial-wave spectroscopic microscopy", *Proc. Natl. Acad. Sci. U.S.A.*, **113** (2016) E6372.

[28] Dempsey G. T., Vaughan J. C., Chen K. H., Bates M. and Zhuang X., "Evaluation of fluorophores for optimal performance in localization-based super-resolution imaging", *Nat. Meth.*, **8** (2011) 1027.

[29] Turkowyd B., Virant D. and Endesfelder U., "From single molecules to life: microscopy at the nanoscale", *Anal. Bioanal. Chem.*, **408** (2016) 6885, http://dx.doi.org/10.1007/s00216-016-9781-8.

[30] Wombacher R., Heidbreder M., van de Linde S., Sheetz M. P., Heilemann M., Cornish V. W. and Sauer M., "Live-cell super-resolution imaging with trimethoprim conjugates", *Nat. Meth.*, **7** (2010) 717.

[31] Flors C., "DNA and chromatin imaging with super-resolution fluorescence microscopy based on single-molecule localization", *Biopolymers*, **95** (2011) 290.

[32] Ebeling D. *et al.*, "Imaging of biomaterials in liquids: a comparison between conventional and Q-controlled amplitude modulation ('tapping mode') atomic force microscopy", *Nanotechnology*, **17** (2006) S221, http://stacks.iop.org/0957-4484/17/i=7/a=S20.

[33] Poma A., Spano L., Pittaluga E., Tucci A., Palladino L. and Limongi T., "Interactions between saporin, a ribosome-inactivating protein, and DNA: a study by atomic force microscopy", *J. Microsc.*, **217** (2005) 69.

[34] Di Bucchianico S., Venora G., Lucretti S., Limongi T., Palladino L. and Poma A., "Saponaria officinalis karyology and karyotype by means of image analyzer and atomic force microscopy", *Microsc. Res. Tech.*, **71** (2008) 730.

[35] Lyubchenko Y. L., Shlyakhtenko L. S. and Ando T., "Imaging of nucleic acids with atomic force microscopy", *Methods*, **54** (2011) 274.

[36] Lyubchenko Y. L., "DNA structure and dynamics: an atomic force microscopy study", *Cell Biochem. Biophys.*, **41** (2004) 75.

[37] Billingsley D. J., Bonass W. A., Crampton N., Kirkham J. and Thomson N. H., "Single-molecule studies of DNA transcription using atomic force microscopy", *Phys. Biol.*, **9** (2012) 21001.

[38] Pyne A., Thompson R., Leung C., Roy D. and Hoogenboom B.W., "Single-molecule reconstruction of oligonucleotide secondary structure by atomic force microscopy", *Small*, **10** (2014) 3257.

[39] Uchihashi T., Tanigawa M., Ashino M., Sugawara Y., Yokoyama K., Morita S. and Ishikawa Mitsuru, "Identification of B-Form DNA in an Ultrahigh Vacuum by Noncontact-Mode Atomic Force Microscopy", *Langmuir*, **16** (2000) 1349.

[40] Ido S., Kimura K., Oyabu N., Kobayashi K., Tsukada M., Matsushige K. and Yamada H., "Beyond the helix pitch: Direct visualization of native DNA in aqueous solution", *ACS Nano*, **7** (2013) 1817.

[41] Tanaka H. and Kawai T., "Partial sequencing of a single DNA molecule with a scanning tunnelling microscope", *Nat. Nanotechnol.*, **4** (2009) 518, http://dx.doi.org/10.1038/nnano.2009.155.

[42] Shapir E., Cohen H., Calzolari A., Cavazzoni C., Ryndyk D. A, Cuniberti G., Kotlyar A., Di Felice R. and Porath D., "Electronic structure of single DNA molecules resolved by transverse scanning tunnelling spectroscopy", *Nat. Mater.*, **7** (2008) 68.

[43] Sun H.B. and Yokota H., "MutS-mediated detection of DNA mismatches using atomic force microscopy", *Anal. Chem.*, **72** (2000) 3138.

[44] Wang H., Yang Y., Schofield M.J., Du C., Fridman Y., Lee S. D., Larson E. D., Drummond J. T., Alani E., Hsieh P. and Erie D. A, "DNA bending and unbending by MutS govern mismatch recognition and specificity", *Proc. Natl. Acad. Sci. U.S.A.*, **100** (2003) 14822, http://www.pubmedcentral.nih.gov/articlerender.fcgi?artid=299810&tool=pmcentrez&rendertype=abstract.

[45] Jiang Y. and Marszalek P. E., "Atomic force microscopy captures MutS tetramers initiating DNA mismatch repair", *Embo J.*, **30** (2011) 2881, http://www.ncbi.nlm.nih.gov/pubmed/21666597%5Cnhttp://emboj.embopress.org/content/embojnl/30/14/2881.full.pdf.

[46] Robin Harris J. and Horne R. W., "Negative staining: A brief assessment of current technical benefits, limitations and future possibilities", *Micron.*, **25** (1994) 5.

[47] Uyeda Y. and Fujiyoshi N., "The Alumina Supermicrogrid for High Resolution Electron Microscopy", *J. Electron. Microsc.*, **27** (1978) 75.

[48] Fujiyoshi Y. and Uyeda N., "Direct imaging of a double-strand DNA molecule", *Ultramicroscopy.*, **7** (1981) 189, http://www.sciencedirect.com/science/article/pii/0304399181900097.

[49] Taylor K. A. and Glaeser R. M., "Electron Diffraction of Frozen, Hydrated Protein Crystals", *Science*, **186** (1974) 1036, http://www.sciencemag.org/content/186/4168/1036.abstract.

[50] Brilot A. F., Chen J. Z., Cheng A., Pan J., Harrison S. C., Potter C. S., Carragher B., Henderson R. and Grigorieff N., "Beam-induced motion of vitrified specimen on holey carbon film", *J. Struct. Biol.*, **177** (2012) 630.

[51] Nogales E., "The development of cryo-EM into a mainstream structural biology technique", *Nat. Meth.*, **13** (2016) 24, http://dx.doi.org/10.1038/nmeth.3694%5Cn10.1038/nmeth.3694.

[52] Nogales E. and Scheres S. H. W., "Cryo-EM: A Unique Tool for the Visualization of Macromolecular Complexity", *Mol. Cell.*, **58** (2015) 677.

[53] Mishyna M., Volokh O., Danilova Y., Gerasimova N., Pechnikova E. and Sokolova O. S., "Effects of radiation damage in studies of protein-DNA complexes by cryo-EM", *Micron.*, **96** (2017) 57, http://linkinghub.elsevier.com/retrieve/pii/S0968432816303626.

[54] Bartesaghi A., Merk A., Banerjee S., Matthies D., Wu X., Milne J. L. S. and Subramaniam S., "2.2 Å resolution cryo-EM structure of β-galactosidase in complex with a cell-permeant inhibitor", *Science*, **348** (2015) 1147, http://www.sciencemag.org.ezproxy.lib.monash.edu.au/content/348/6239/1147.abstract.

[55] Banerjee S., Bartesaghi A., Merk A., Rao P., Bulfer S. L., Yan Y., Green N., Mroczkowski B., Neitz R. J., Wipf P., Falconieri V., Deshaies R. J., Milne J. L. S., Huryn D., Arkin M. and Subramaniam S., "2.3 Å resolution cryo-EM structure of human p97 and mechanism of allosteric inhibition", *Science*, **351** (2016) 871, http://science.sciencemag.org/content/early/2016/01/27/science.aad7974.abstract%5Cnhttp://www.sciencemag.org/cgi/doi/10.1126/science.aad7974%5Cnhttp://arxiv.org/abs/1011.1669%5Cnhttp://dx.doi.org/10.1088/1751-8113/44/8/085201%5Cnhttp://stacks.iop.org/1751-8121/44.

[56] Henderson R. and Glaeser R. M., "Quantitative analysis of image contrast in electron micrographs of beam-sensitive crystals", *Ultramicroscopy*, **16** (1985) 139.

[57] Typke D., Gilpin C. J., Downing K. H. and Glaeser R. M., "Stroboscopic image capture: Reducing the dose per frame by a factor of 30 does not prevent beam-induced specimen movement in paraffin", *Ultramicroscopy*, **107** (2007) 106.

[58] Li X., Mooney P., Zheng S., Booth C. R., Braunfeld M. B., Gubbens S., Agard D. A. and Cheng, Y., "Electron counting and beam-induced motion correction enable near-atomic-resolution single-particle cryo-EM", *Nat. Methods*, **10** (2013) 584, http://www.nature.com/doifinder/10.1038/nmeth.2472%5Cnhttp://www.ncbi.nlm.nih.gov/pubmed/23644547%5Cnhttp://www.pubmedcentral.nih.gov/articlerender.fcgi?artid=PMC3684049.

[59] Song F., Chen P., Sun D., Wang M., Dong L., Liang D., Xu R. M., Zhu P. and Li G., "Cryo-EM study of the chromatin fiber reveals a double helix twisted by tetranucleosomal units", *Science*, **344** (2014) 376, http://www.ncbi.nlm.nih.gov/pubmed/24763583.

[60] Sun M., Luo C., Xu L., Ji H., Ouyang Q., Yu D. and Chen Y., "Artificial lotus leaf by nanocasting", *Langmuir*, **21** (2005) 8978.

[61] Barthlott W. and Neinhuis C., "Purity of the sacred lotus, or escape from contamination in biological surfaces", *Planta*, **202** (1997) 1.

[62] Wagner T., Neinhuis C. and Barthlott W., "Wettability and Contaminability of Insect Wings as a Function of Their Surface Sculptures", *Acta Zool.*, **77** (1996) 213, http://doi.wiley.com/10.1111/j.1463-6395.1996.tb01265.x.

[63] Wenzel R. N., "Resistance of solid surfaces to wetting by water", *J. Ind. Eng. Chem. (Washington, D. C.)*, **28** (1936) 988.

[64] Cassie B. D., Cassie A. B. D. and Baxter S., "Wettability of porous surfaces", *Trans. Faraday Soc.*, **40** (1944) 546.

[65] Cassie A. B. D. and Baxter S., "Large Contact Angles of Plant and Animal Surfaces", *Nature*, **155** (1945) 21, http://adsabs.harvard.edu/abs/1945Natur.155...21C.

[66] De Angelis F., Gentile F., Mecarini F., Das G., Moretti M., Candeloro P., Coluccio M. L., Cojoc G., Accardo A., Liberale C., Zaccaria R. P., Perozziello G., Tirinato L., Toma A., Cuda G., Cingolani R. and Di Fabrizio E., "Breaking the diffusion limit with super-hydrophobic delivery of molecules to plasmonic nanofocusing SERS structures", *Nat. Photon.*, **5** (2011) 682.

[67] Ciasca G., Papi M., Businaro L., Campi G., Ortolani M., Palmieri V., Cedola A., De Ninno A., Gerardino A., Maulucci G. and De Spirito M., "Recent advances in superhydrophobic surfaces and their relevance to biology and medicine", *Bioinspir. Biomim.*, **11** (2016) 11001.

[68] Draper M. C., Crick C. R., Orlickaite V., Turek V. A., Parkin I. P. and Edel J. B., "Superhydrophobic surfaces as an on-chip microfluidic toolkit for total droplet control", *Anal. Chem.*, **85** (2013) 5405.

[69] Quéré D., "Non-sticking drops", *Rep. Prog. Phys.*, **68** (2005) 2495.

[70] Peng L., Li H., Zhang Y., Su J., Yu P. and Luo Y., "A superhydrophobic 3D porous material for oil spill cleanup", *RSC Adv.*, **4** (2014) 46470.

[71] Gentile F., Das G., Coluccio M. L., Mecarini F., Accardo A., Tirinato L., Tallerico R., Cojoc G., Liberale C., Candeloro P., Decuzzi P., De Angelis F. and Di Fabrizio E., "Ultra low concentrated molecular detection using super hydrophobic surface based biophotonic devices", *Microelectron. Eng.*, **87** (2010) 798, http://dx.doi.org/10.1016/j.mee.2009.11.083.

[72] Marini M., Das G., La Rocca R., Gentile F., Limongi T., Santoriello S., Scarpellini A. and Di Fabrizio E., "Raman spectroscopy for detection of stretched DNAs on superhydrophobic surfaces", *Microelectron. Eng.*, **119** (2014) 151, http://dx.doi.org/10.1016/j.mee.2014.04.008.

[73] Marini M., Falqui A., Moretti M., Limongi T., Allione M., Genovese A., Lopatin S., Tirinato L., Das G., Torre B., Giugni A., Gentile F., Candeloro P. and Di

Fabrizio E., "The structure of DNA by direct imaging", *Sci. Adv.*, **1** (2015) e1500734, http://advances.sciencemag.org/content/1/7/e1500734.abstract.

[74] Gentile F., Coluccio M. L., Accardo A., Asande M., Cojoc G., Mecarini F., Das G., Liberale C., De Angelis F., Candeloro P., Decuzzi P. and Di Fabrizio E., "Nanoporous-micropatterned-superhydrophobic surfaces as harvesting agents for few low molecular weight molecules", *Microelectron. Eng.*, **88** (2011) 1749, http://dx.doi.org/10.1016/j.mee.2010.12.076.

[75] Gentile F., Coluccio M. L., Rondanina E., Santoriello S., Di Mascolo D., Accardo A., Francardi M., De Angelis F., Candeloro P. and Di Fabrizio E., "Non periodic patterning of super-hydrophobic surfaces for the manipulation of few molecules", *Microelectron. Eng.*, **111** (2013) 272, http://dx.doi.org/10.1016/j.mee.2013.01.036.

[76] Miele E., Accardo A., Falqui A., Marini M., Giugni A., Leoncini M., De Angelis F., Krahne R. and Di Fabrizio E., "Writing and functionalisation of suspended DNA nanowires on superhydrophobic pillar arrays", *Small*, **11** (2015) 134.

[77] Accardo A., Tirinato L., Altamura D., Sibillano T., Giannini C., Riekel C. and Di Fabrizio E., "Superhydrophobic surfaces allow probing of exosome self organization using X-ray scattering", *Nanoscale*, **5** (2013) 2295-9, http://www.ncbi.nlm.nih.gov/pubmed/23426504.

[78] Accardo A., Di Fabrizio E., Limongi T., Marinaro G. and Riekel C., "Probing droplets on superhydrophobic surfaces by synchrotron radiation scattering techniques", *J. Synchrotron Radiat.*, **21** (2014) 643.

[79] Gentile F., Moretti M., Limongi T., Falqui A., Bertoni G., Scarpellini A., Santoriello S., Maragliano L., Proietti Zaccaria R. and Di Fabrizio E., "Direct imaging of DNA fibers: The visage of double helix", *Nano Lett.*, **12** (2012) 6453.

[80] Gentile F., Coluccio M. L., Limongi T., Perozziello G., Candeloro P. and Di Fabrizio E., "The five Ws (and one H) of super-hydrophobic surfaces in medicine", *Micromachines.*, **5** (2014) 239.

[81] Gentile F., Battista E., Accardo A., Coluccio M. L., Asande M., Perozziello G., Das G., Liberale C., De Angelis F., Candeloro P., Decuzzi P. and Di Fabrizio E., "Fractal structure can explain the increased hydrophobicity of nanoporous silicon films", *Microelectron. Eng.*, **88** (2011) 2537, http://dx.doi.org/10.1016/j.mee.2011.01.046.

[82] Gentile F., Coluccio M. L., Accardo A., Marinaro G., Rondanina E., Santoriello S., Marras S., Das G., Tirinato L., Perozziello G., De Angelis F., Dorigoni C., Candeloro P. and Di Fabrizio E., "Tailored Ag nanoparticles/nanoporous superhydrophobic surfaces hybrid devices for the detection of single molecule", *Microelectron. Eng.*, **97** (2012) 349, http://dx.doi.org/10.1016/j.mee.2012.03.025.

[83] Gentile F., Coluccio M. L., Coppede N., Mecarini F., Das G., Liberale C., Tirinato L., Leoncini M., Perozziello G., Candeloro P., De Angelis F. and Di Fabrizio E., "Superhydrophobic surfaces as smart platforms for the analysis of diluted biological solutions", *ACS Appl. Mater. Interfaces*, **4** (2012) 3213.

[84] Sanger F., Coulson A. R., Hong G. F., Hill D. F. and Petersen G. B., "Nucleotide sequence of bacteriophage lambda DNA", *J. Mol. Biol.*, **162** (1982) 729.

[85] Daniels D. L., Schroeder J. L., Szybalski W., Sanger F., Coulson A. R., Hong G. F., Hill D. F., Petersen G. B. and Blattner F. R., *"APPENDIX II Complete Annotated Lambda Sequence"*, (1983).

[86] Gentile F., Coluccio M. L., Limongi T., Perozziello G., Candeloro P. and Di Fabrizio E., "The five Ws (and one H) of super-hydrophobic surfaces in medicine", *Micromachines*, **5** (2014) 239.

[87] Williams D. B. and Carter C. B., Transmission Electron Microscopy: *A Textbook for Materials Science*, 2nd edition (Springer-Verlag, New York) 2009, http://www.loc.gov/catdir/enhancements/fy0820/96028435-d.html.

[88] Voet D. and Rich A., "The crystal structures of purines, pyrimidines and their intermolecular complexes", *Prog. Nucleic Acid Res.*, **10** (1970) 183.

[89] Marini M., Limongi T., Falqui A., Genovese A., Allione M., Moretti M., Lopatin S., Tirinato L., Das G., Torre B., Giugni A., Cesca F., Benfenati F. and Di Fabrizio E., "Imaging and structural studies of DNA-protein complexes and membrane ion channels", *Nanoscale*, **9** (2016) 2768.

[90] Marini M., Limongi T., Allione M., Falqui A. and E D. F., "Superhydrophobic Manipulation of DNA", *Adv. Gen. Eng.*, **3** (2014) 10, http://www.omicsgroup.org/journals/cardiac-specific-knockout-of-p65-mice-resist-to-cardiac-ischemiareperfusion-injury-2169-0111-1000i101.php?aid=42891.

[91] Marini M., Allione M., Torre B., Moretti M., Limongi T., Tirinato L., Giugni A., Das G. and di Fabrizio E., "Raman on suspended DNA: Novel superhydrophobic approach for structural studies", *Microelectron. Eng.*, **175** (2017) 38, http://linkinghub.elsevier.com/retrieve/pii/S0167931716305275.

[92] Theophanides T. and Tajmir-Riahi H. A., "Flexibility of DNA and RNA upon Binding to Different Metal Cations. An Investigation of the B to A to Z Conformational Transition by Fourier Transform Infrared Spectroscopy", *J. Biomol. Struct. Dyn.*, **2** (1985) 995, http://dx.doi.org/10.1080/07391102.1985.10507615.

[93] Parker F. S., "Crystal and solution structures of the B-DNA dodecamer d(CGCAAATTTGCG) probed by Raman spectroscopy: heterogeneity in the crystal structure does not persist in the solution structure", *Biochemistry*, **27** (1988) 931, http://www.ncbi.nlm.nih.gov/pubmed/3365372.

[94] Parker F. S., "Applications of infrared, Raman and resonance Raman spectroscopy in biochemistry", *J. Mol. Struct.*, **128** (1985) 349, http://www.sciencedirect.com/science/article/pii/0022286085850122.

[95] Gentile F., Coluccio M. L., Toma A., Alabastri A., Zaccaria R. P., Das G., De Angelis F., Candeloro P., Liberale C., Perozziello G., Tirinato L., Leoncini M. and Di Fabrizio E., "Plasmonics and Super-Hydrophobicity: A New Class of Nano-Bio-Devices", *Plasmon. Theory Appl.*, **15** (2013) 501.

[96] Das G., Gentile F., De Angelis F., Coluccio M. L., Liberale C., Proietti Zaccaria R. and Di Fabrizio E., Superhydrophobicity, plasmonics and Raman spectroscopy for few/single molecule detection down to attomolar concentration, *Proc. SPIE*, **8457** (2012) 84570C, http://proceedings.spiedigitallibrary.org/proceeding.aspx?doi=10.1117/12.936517.

[97] Coluccio M. L., Gentile F., Das G., Nicastri A., Perri A. M., Candeloro P., Perozziello G., Proietti Zaccaria R., Gongora J. S. T., Alrasheed S., Fratalocchi A., Limongi T., Cuda G. and Di Fabrizio E., "Detection of single amino acid mutation in human breast cancer by disordered plasmonic self-similar chain", *Sci. Adv.*, **1** (2015) e1500487.

[98] Gentile F., Coluccio M. L., Zaccaria R. P., Francardi M., Cojoc G., Perozziello G., Raimondo R., Candeloro P. and Di Fabrizio E., "Selective on site separation and detection of molecules in diluted solutions with super-hydrophobic clusters of plasmonic nanoparticles", *Nanoscale*, **6** (2014) 8208, http://pubs.rsc.org/en/content/articlelanding/2014/nr/c4nr00796d%5Cnhttp://pubs.rsc.org/en/content/articlelanding/2014/nr/c4nr00796d#!divAbstract.

[99] De Angelis F., Das G., Candeloro P., Patrini M., Galli M., Bek A., Lazzarino M., Maksymov I., Liberale C., Andreani L. C. and Di Fabrizio E., "Nanoscale chemical mapping using three-dimensional adiabatic compression of surface plasmon polaritons", *Nat. Nanotechnol.*, **5** (2010) 67, http://dx.doi.org/10.1038/nnano.2009.348.

[100] Tirinato L., Gentile F., Di Mascolo D., Coluccio M. L., Das G., Liberale C., Pullano S. A., Perozziello G., Francardi M., Accardo A., De Angelis F., Candeloro P. and Di Fabrizio E., "SERS analysis on exosomes using superhydrophobic surfaces", *Microelectron. Eng.*, **97** (2012) 337, http://dx.doi.org/10.1016/j.mee.2012.03.022.

[101] Hood J. L., San Roman S. and Wickline S. A., "Exosomes released by melanoma cells prepare sentinel lymph nodes for tumor metastasis", *Cancer Res.*, **71** (2011) 3792.

[102] Lee T. H., D'Asti E., Magnus N., Al-Nedawi K., Meehan B. and Rak J., "Microvesicles as mediators of intercellular communication in cancer-the emerging science of cellular "debris"", *Semin. Immunopathol.*, **33** (2011) 1.
[103] Dawson T. M. and Dawson V. L., "Molecular pathways of neurodegeneration in Parkinson's disease", *Science*, **302** (2003) 819.
[104] Crews L. and Masliah E., "Molecular mechanisms of neurodegeneration in Alzheimer's disease", *Human Mol. Genet.*, **19** (2010) R12.
[105] Kelly J. W., "Amyloid fibril formation and protein misassembly: a structural quest for insights into amyloid and prion diseases", *Structure*, **5** (1997) 595, http://www.sciencedirect.com/science/article/pii/S0969212697002153%5Cnhttp://www.ncbi.nlm.nih.gov/pubmed/9195890.
[106] Pepys M. B., Hawkins P. N., Booth D. R., Vigushin D. M., Tennent G. A., Soutar A. K., Totty N., Nguyen O., Blake C. C. F., Terry C. J., Feest T. G., Zalin A. M. and Hsuan J. J., "Human Lysozyme Gene-Mutations Cause Hereditary Systemic Amyloidosis", *Nature*, **362** (1993) 553.
[107] Lakshmanan A., Cheong D. W., Accardo A., Di Fabrizio E., Riekel C. and Hauser C. A. E., "Aliphatic peptides show similar self-assembly to amyloid core sequences, challenging the importance of aromatic interactions in amyloidosis", *Proc. Natl. Acad. Sci. U.S.A.*, **110** (2013) 519, http://www.pnas.org/content/110/2/519.
[108] Accardo A., Gentile F., Mecarini F., De Angelis F., Burghammer M., Di Fabrizio E. and Riekel C., "In situ X-ray scattering studies of protein solution droplets drying on micro-and nanopatterned superhydrophobic PMMA surfaces", *Langmuir*, **26** (2010) 15057.
[109] Accardo A., Burghammer M., Di Cola E., Reynolds M., Di Fabrizio E. and Riekel C., "Lysozyme fibrillation induced by convective flow under quasi contact-free conditions", *Soft Matter.*, **7** (2011) 6792, http://pubs.rsc.org/en/content/articlehtml/2011/sm/c1sm05783a.
[110] Limongi T., Cesca F., Gentile F., Marotta R., Ruffilli R., Barberis A., Dal Maschio M., Petrini E. M., Santoriello S., Benfenati F. and Di Fabrizio E., "Nanostructured superhydrophobic substrates trigger the development of 3D neuronal networks", *Small*, **9** (2013) 402.
[111] Cesca F., Limongi T., Accardo A., Rocchi A., Orlando M., Shalabaeva V., Di Fabrizio E. and Benfenati F., "Fabrication of biocompatible free-standing nanopatterned films for primary neuronal cultures", *RSC Adv.*, **4** (2014) 45696, http://pubs.rsc.org/en/content/articlehtml/2014/ra/c4ra08361j.
[112] Egerton R. F., Li P. and Malac M., "Radiation damage in the TEM and SEM", *Micron*, **35** (2004) 399.
[113] Egerton R. F., "Mechanisms of radiation damage in beam-sensitive specimens, for TEM accelerating voltages between 10 and 300 kV", *Microsc. Res. Tech.*, **75** (2012) 1550.
[114] Eastman A., "The formation, isolation and characterization of DNA adducts produced by anticancer platinum complexes", *Pharmacol. Ther.*, **34** (1987) 155.
[115] Wang D. and Lippard S. J., "Cellular processing of platinum anticancer drugs", *Nat. Rev. Drug Deliv.*, **4** (2005) 307.
[116] Ono A., Cao S., Togashi H., Tashiro M., Fujimoto T., Machinami T., Oda S., Miyake Y., Okamoto I. and Tanaka Y., "Specific interactions between silver(I) ions and cytosine-cytosine pairs in DNA duplexes", *Chem. Commun. (Cambridge)*, Issue 39 (2008) 4825.
[117] Singer-Lahat D., Dascal N., Mittelman L., Peleg S. and Lotan I., "Imaging plasma membrane proteins in large membrane patches of Xenopus oocytes", *Pflugers Arch. Eur. J. Physiol.*, **440** (2000) 627.
[118] Navas P., Nowack D. D. and Morre D. J., "Isolation of purified plasma membranes from cultured cells and hepatomas by two-phase partition and preparative free-flow electrophoresis", *Cancer Res.*, **49** (1989) 2147.
[119] Sereda V. and Lednev I. K., "Polarized Raman spectroscopy of aligned insulin fibrils", *J. Raman Spectrosc.*, **45** (2014) 665.

[120] Jahn T. R., Makin O. S., Morris K. L., Marshall K. E., Tian P., Sikorski P. and Serpell L. C., "The common architecture of cross-beta amyloid", *J. Mol. Biol.*, **395** (2010) 717, http://www.ncbi.nlm.nih.gov/pubmed/19781557.

[121] Van Dyck D. and Chen F.-R., "'Big Bang' tomography as a new route to atomic-resolution electron tomography", *Nature*, **486** (2012) 243, http://www.ncbi.nlm.nih.gov/pubmed/22699616.

[122] Ophus C., Ciston J., Pierce J., Harvey T. R., Chess J., McMorran B. J., Czarnik C., Rose H. H. and Ercius P., "Efficient linear phase contrast in scanning transmission electron microscopy with matched illumination and detector interferometry", *Nat. Commun.*, **7** (2016) 10719, http://www.nature.com/ncomms/2016/160229/ncomms10719/full/ncomms10719.html.

[123] Mohri K., Kusuki E., Ohtsuki S., Takahashi N., Endo M., Hidaka K., Sugiyama H., Takahashi Y., Takakura Y. and Nishikawa M., "Self-Assembling DNA Dendrimer for Effective Delivery of Immunostimulatory CpG DNA to Immune Cells", *Biomacromolecules*, **16** (2015) 1095.

[124] Marini M., Piantanida L., Musetti R., Bek A., Dong M., Besenbacher F., Lazzarino M. and Firrao G., "A revertible, autonomous, self-assembled DNA-origami nanoactuator", *Nano Lett.*, **11** (2011) 5449, http://www.ncbi.nlm.nih.gov/pubmed/22047682.

[125] Piantanida L., Naumenko D., Torelli E., Marini M., Bauer D. M., Fruk L., Firrao G. and Lazzarino M., "Plasmon resonance tuning using DNA origami actuation", *Chem. Commun.*, **51** (2015) 4789.

[126] Torelli E., Marini M., Palmano S., Piantanida L., Polano C., Scarpellini A., Lazzarino M. and Firrao G., "A DNA origami nanorobot controlled by nucleic acid hybridization", *Small*, **10** (2014) 2918.

[127] Yan H., Zhang X., Shen Z. and Seeman N. C., "A robust DNA mechanical device controlled by hybridization topology", *Nature*, **415** (2002) 62.

[128] Manuscript A. and Malignancies H., "Detection of Circulating Tumor DNA in Early- and Late-Stage Human Malignancies", *Sci. Transl. Med.*, **6** (2014) 224ra24.

[129] Gray E. S., Rizos H., Reid A. L., Boyd S. C., Pereira M. R., Lo J., Tembe V., Freeman J., Lee J. H. J., Scolyer R. A., Siew K., Lomma C., Cooper A., Khattak M. A., Meniawy T. M. Long, G. V., Carlino M. S., Millward M. and Ziman M., "Circulating tumor DNA to monitor treatment response and detect acquired resistance in patients with metastatic melanoma", *Oncotarget*, **6** (2015) 42008, http://www.pubmedcentral.nih.gov/articlerender.fcgi?artid=4747205&tool=pmcentrez&rendertype=abstract.

[130] Aarthy R., Mani S., Velusami S., Sundarsingh S. and Rajkumar T., "Role of Circulating Cell-Free DNA in Cancers", *Mol. Diagnosis Ther.*, **19** (2015) 339.

[131] Bellassai N. and Spoto G., "Biosensors for liquid biopsy: circulating nucleic acids to diagnose and treat cancer", *Anal. Bioanal. Chem.*, **408** (2016) 1.

[132] Dinakaran V., Rathinavel A., Pushpanathan M., Sivakumar R., Gunasekaran P. and Rajendhran J., "Elevated levels of circulating DNA in cardiovascular disease patients: metagenomic profiling of microbiome in the circulation", *PLoS One.*, **9** (2014) e105221.

[133] Bakir M., Engin A., Kuskucu M. A., Bakir S., Gündag O. and Midilli K., "Relationship of Plasma Cell-Free DNA Level With Mortality and Prognosis in Patients With Crimean–Congo Hemorrhagic Fever", *J. Med. Virol.*, **88** (2016) 1152.

[134] Basak R., Nair N. K. and Mittra I., "Evidence for cell-free nucleic acids as continuously arising endogenous DNA mutagens", *Mutat. Res. Mol. Mech. Mutagen.*, **793** (2016) 15, http://dx.doi.org/10.1016/j.mrfmmm.2016.10.002.